

A Test of Spectroscopic Age Estimates of White Dwarfs using Wide WD+WD Binaries

TYLER M. HEINTZ ,¹ J. J. HERMES ,¹ P.-E. TREMBLAY ,² LOU BAYA OULD ROUIS ,¹ JOSHUA S. REDING ,³
 B. C. KAISER ,³ AND JENNIFER L. VAN SADERS ⁴

¹Department of Astronomy & Institute for Astrophysical Research, Boston University, 725 Commonwealth Ave, Boston, MA, 02215, USA

²Department of Physics, University of Warwick, Coventry, CV4 7AL, UK

³Department of Physics and Astronomy, University of North Carolina at Chapel Hill, Chapel Hill, NC 27599, USA

⁴Institute for Astronomy, University of Hawai'i, 2680 Woodlawn Drive, Honolulu, HI 96822, USA

ABSTRACT

White dwarf stars have been used for decades as precise and accurate age indicators. This work presents a test of the reliability of white dwarf total ages when spectroscopic observations are available. We conduct follow-up spectroscopy of 148 individual white dwarfs in widely separated double-white-dwarf (WD+WD) binaries. We supplement the sample with 264 previously published white dwarf spectra, as well as 1292 high-confidence white dwarf spectral types inferred from their Gaia XP spectra. We find that spectroscopic fits to optical spectra do not provide noticeable improvement to the age agreement among white dwarfs in wide WD+WD binaries. The median age agreement is $\approx 1.5\sigma$ for both photometrically and spectroscopically determined total ages, for pairs of white dwarfs with each having a total age uncertainty $< 20\%$. For DA white dwarfs, we further find that photometrically determined atmospheric parameters from spectral energy distribution fitting give better total age agreement (1.0σ , 0.2 Gyr, or 14% of the binary's average total age) compared to spectroscopically determined parameters from Balmer-line fits (agreement of 1.5σ , 0.3 Gyr, or 28% of binary's average total age). We find further evidence of a significant merger fraction among wide WD+WD binaries: across multiple spectroscopically identified samples, roughly 20% are inconsistent with a monotonically increasing initial-final mass relation. We recommend the acquisition of an identification spectrum to ensure the correct atmospheric models are used in photometric fits in order to determine the most accurate total age of a white dwarf star.

Keywords: white dwarfs, binary stars, ages, spectroscopy

1. INTRODUCTION

Stellar age is a notoriously difficult parameter to measure, especially for stars that experience little observable evolution in a color-magnitude diagram (CMD) over their lifetimes. The ages of field stars are vital for understanding the evolution of stellar and galactic systems, but there is no single method suitable for the wide range of stellar types observed. Thus, stellar ages are determined through a variety of indirect methods, including their position on the CMD (isochrone fitting, e.g., Berger et al. 2018, Xiang & Rix 2022), rotation periods (gyrochronology, e.g., Barnes 2007, Metcalfe &

Egeland 2019, Clayton et al. 2020), activity (e.g., Mamajek & Hillenbrand 2008), stellar pulsations (asteroseismology, e.g., Chaplin et al. 2014), and kinematic properties (e.g., Holmberg et al. 2009; Cheng et al. 2019, Lu et al. 2021). The method most widely used to determine precise stellar ages is isochrone fitting to stellar clusters (e.g., Cummings & Kalirai 2018), which provides the most direct way of measuring stellar ages. Unfortunately this method cannot be widely applied to stars in the field, especially cool main-sequence stars, but can be used as a calibrator for the previously mentioned techniques.

All previously mentioned methods can only be applied to specific classes of stars and are not universally useful. Isochrone fitting is most useful for populations of stars born at the same time or stars that experience relatively rapid evolution on the CMD (e.g., subgiant stars, Xi-

Corresponding author: Tyler M. Heintz
 tmheintz@bu.edu

ang & Rix 2022). Gyrochronology works well for young and intermediate-mass solar-type stars, as their rotations are slowed through interactions with their stellar winds (Skumanich 1972), but becomes less effective in old Sun-like stars (van Saders et al. 2016) that undergo weakened magnetic braking, and in low-mass stars at a wide range of ages that undergo core-envelope decoupling (Lanzafame et al. 2019; Curtis et al. 2020). It fails entirely in stars without convective envelopes (Kraft 1967).

White dwarf stars are ubiquitous throughout the Galaxy and are the final endpoint of 97% of all stars (Fontaine et al. 2001). Their relatively simple and characteristic cooling allows for accurate and precise age determinations through robust cooling models (e.g., Bédard et al. 2020). Their total ages (the combined time as a white dwarf and the time in the main-sequence and giant phases) can be inferred through the use of an initial-final mass relation (IFMR, Weidemann & Koester 1983; Catalán et al. 2008; Kalirai et al. 2008; Salaris et al. 2009; Williams et al. 2009; Cummings et al. 2018; Cunningham et al. 2024), which relates the zero-age main-sequence (ZAMS) mass to the final white dwarf mass in tandem with stellar evolutionary grids (e.g., MESA, Dotter 2016). Thus, white dwarfs both serve as additional calibrators to the methods mentioned previously (e.g. Rebassa-Mansergas et al. 2023) and provide an understanding of the limitations of white dwarf total ages. These are crucial for their future use as stellar age indicators.

The total age of a white dwarf is strongly dependent on how much mass it lost during its giant phase, and thus the IFMR chosen, especially for the lowest-mass white dwarfs ($M < 0.63 M_{\odot}$). The IFMR is poorly constrained at these low masses due to the lack of white dwarfs with lower-than-average masses in observable stellar clusters. This problem has been investigated using both white dwarfs in wide binaries (Zhao et al. 2012; Barrientos & Chanamé 2021; Hollands et al. 2024) and the distribution of white dwarfs in the CMD (El-Badry et al. 2018; Cunningham et al. 2024). However, the resulting IFMRs from these studies provide a wide range of predicted initial masses, especially for lower-mass white dwarfs. The IFMR is also likely affected by the initial rotation and metallicity of the white dwarf progenitors (Cummings et al. 2019).

With the advent of the Gaia mission (Gaia Collaboration et al. 2016, 2018, 2021), samples of widely separated binaries have increased by an order of magnitude (Andrews et al. 2015; El-Badry & Rix 2018; Tian et al. 2020). In Gaia Early Data Release 3 (EDR3), El-Badry et al. (2021) found more than a million wide (>100 au

separation) binaries. These wide binaries provide unique opportunities to test the levels of precision and accuracy obtainable from white dwarf total ages.

In El-Badry et al. (2021), there are more than 18,000 high-confidence wide white dwarf plus main-sequence binaries (WD+MS). Previous work used white dwarfs in wide binaries to constrain the ages of their binary companions (e.g., Fouesneau et al. 2019, Qiu et al. 2021). These works provide large catalogs (92 and 4050, respectively) of stellar ages derived from coeval white dwarf companions using their available broad-band photometry. To fully realize the potential of the large sample of wide WD+MS binaries from El-Badry et al. (2021), a thorough understanding of the accuracy and precision achievable with white dwarf total ages is needed.

In a previous study (Heintz et al. 2022), we tested the accuracy and precision of white dwarf total ages using the sample of more than 1500 widely separated double-white-dwarf binaries (WD+WD) from El-Badry et al. (2021), as well as two dozen new triple systems with at least two white dwarfs. In that work, we used broad-band photometry to determine the total ages of the white dwarfs. We found that roughly 20 – 35% of wide WD+WD binaries showed more massive white dwarfs to have shorter cooling ages than their wide companions, implying that the less massive white dwarf came from a more massive main-sequence star, which is inconsistent with the current model of a monotonically increasing IFMR. With only photometric data available for the majority of the sample, it was difficult to determine the exact reason for these discrepancies. We aim to test here whether spectroscopic observations can help illuminate the intrinsic causes of the previously found discrepancies.

In recent years, there has been evidence of disagreements between atmospheric parameters derived from photometry and spectroscopy (Tremblay et al. 2019; Bergeron et al. 2019; Gentile Fusillo et al. 2021; O'Brien et al. 2023; Sahu et al. 2023). The disagreement for an individual white dwarf can be on the order of a few percent in temperature and on the order of 0.1 dex in surface gravity ($\log g$). Although these disagreements appear marginal, they can translate into large differences in derived total ages for individual white dwarfs, especially for the lowest-mass white dwarfs where the progenitor lifetime is a steep function with respect to mass.

In this work, we present follow-up spectroscopy for 148 individual white dwarfs in wide WD+WD binaries along with previously published spectroscopic observations of 264 individual white dwarfs, and investigate the effects on the accuracy and precision of their derived to-

tal ages compared to photometrically determined ages. Section 2 presents the observations and reduction steps, Section 3 discusses the methods used to determine the white dwarf atmospheric parameters and ages, Section 4 presents comparisons of the derived atmospheric parameters and ages from photometry and spectroscopy, and Section 5 summarizes and discusses the implications of this work.

2. OBSERVATIONS AND REDUCTION

2.1. LDT+DeVeny Spectroscopy

We obtained follow-up, low-resolution optical spectra over 12 nights of 84 individual white dwarfs in wide WD+WD binaries with the DeVeny Spectrograph (Bida et al. 2014) on the 4.1-m Lowell Discovery Telescope (LDT) in Happy Jack, Arizona, United States. We used a 300 line mm⁻¹ grating with a 3-arcsec slit, which resulted in wavelength coverage from 3500 – 7000 Å and a seeing-limited resolution, typically 13 – 15 Å.

For the LDT observations, we were restricted to sufficiently separated systems ($\gtrsim 3$ arcseconds) and sufficiently bright targets ($G \lesssim 19.0$ mag) to obtain enough signal to perform spectroscopic fits. In addition, observations were not always collected at the parallactic angle; instead when both stars were in the field of view, we rotated the slit to the appropriate position angle to capture spectra of both white dwarfs simultaneously, substantially cutting our acquisition time. LDT+DeVeny does not have an atmospheric dispersion corrector (ADC), so we planned our observations to occur when the slit position angle was as close to the parallactic angle as possible. A log of our observations is shown in Table B1.

The LDT observations were reduced and the spectra were optimally extracted using the spectroscopic data reduction pipeline PypeIt (Prochaska et al. 2020). A flexure correction is applied using available sky lines in the spectra. The 1-D spectra extracted from each exposure were co-added to be fit for atmospheric parameters (see Section 3.1). We observed one flux standard per night from the ESO X-Shooter spectrophotometric standard stars to flux calibrate the spectra.

2.2. SOAR+Goodman Spectroscopy

For our southern targets, we obtained follow-up optical spectra over 17 nights of 64 individual white dwarfs in wide WD+WD binaries using the Goodman High-Throughput Spectrograph (Clemens et al. 2004) on the 4.1-m Southern Astrophysical Research (SOAR) Telescope located at Cerro Pachón, Chile. We used the 930 line mm⁻¹ grating with grating and camera angles of 13.0 and 24.0 degrees, respectively, which yield a wave-

length coverage of 3600 – 5200 Å. We used slit widths of 1.0 arcsecond and 3.2 arcseconds depending on seeing or weather conditions. The 1.0-arcsecond slit setup resulted in a resolution of 3 Å, while the resolution for the 3.2-arcsecond slit was seeing-limited, resulting in resolutions ranging from 3.5 – 8 Å. Observations are detailed in Table B1.

As with our LDT+DeVeny observations, we often rotated our slit during SOAR+Goodman observations in order to simultaneously capture both white dwarfs when possible. In these cases we used the ADC on SOAR (Briceño et al. 2018), minimizing color-dependent slit losses that could negatively affect flux calibration. We selected targets for this follow-up randomly from the observable wide WD+WD binary sample from El-Badry & Rix (2018).

The SOAR+Goodman observations were also reduced and optimally extracted using the same spectroscopic data reduction pipeline PypeIt (Prochaska et al. 2020) mentioned in Section 2.1. For the SOAR observations, no flexure correction is applied since there are not sufficient sky lines in the wavelength range observed. Thus, the wavelength solutions are unreliable and likely are systematically shifted. This should not affect our fitting described in Section 3.1 since the radial velocity of the white dwarf is a free parameter that can account for these systematic shifts. We adapted the existing `soar_goodman_red` and `soar_goodman_blue` PypeIt classes for our setup, which are suited for the 400 line mm⁻¹ grating. The only change to the classes was to not use the template wavelength solution for the 400 line mm⁻¹ grating, and instead use the “holy-grail” algorithm in PypeIt to generate the wavelength solution for our 930 line mm⁻¹ setup.

2.3. Spectral Types

With the 148 extracted LDT and SOAR spectra, we determine the spectral type of each white dwarf by visual inspection. We find that 104 (67%) are hydrogen-dominated (DA) white dwarfs, one (0.7%) is a helium-dominated (DB) white dwarf, 34 (23%) exhibit flat continua (DC), three (2%) are metal-polluted (DAZ/DZ) white dwarfs, six (4%) are magnetic hydrogen-dominated (DAH) white dwarfs, and one (0.7%) is a carbon-dominated (DQ) white dwarf. As a comparison, in the volume-limited 40 pc sample (O’Brien et al. 2024), 50% are DA white dwarfs, 0.8% are DB white dwarfs, 27% are DC white dwarfs, 11% show metal-pollution, 6% are DAH white dwarfs, and 4% are DQ white dwarfs. Our sample is more similar to a magnitude-limited sample; in Kleinman et al. (2013), 65% are DA white dwarfs, 4.7% are DB white dwarfs,

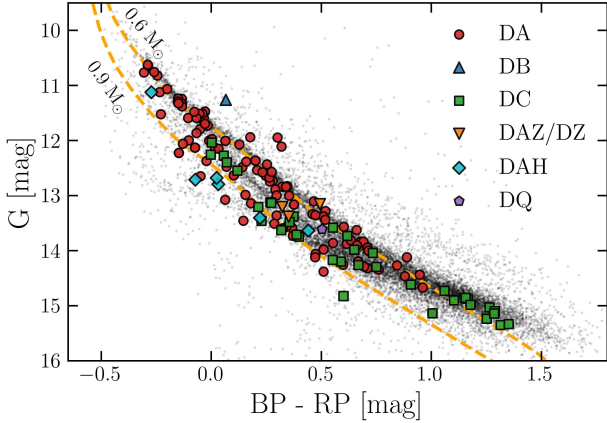


Figure 1. A Gaia CMD with spectral types of the newly observed white dwarfs taken from LDT and SOAR spectra. The grey points in the background are a sample of white dwarfs within 100 pc from [Gaia Collaboration et al. \(2021\)](#) with $<5\%$ parallax uncertainties. The yellow dashed curves are white dwarf cooling sequences for a $0.6 M_{\odot}$ and $0.9 M_{\odot}$ DA white dwarf from [Bédard et al. \(2020\)](#)

2.8% are DC white dwarfs, 2% are metal-polluted, 3.2% are DAH white dwarfs, and 1.1% are DQ white dwarfs. The sample in [Kleinman et al. \(2013\)](#) from the Sloan Digital Sky Survey (SDSS) is biased towards bluer objects, which explains the discrepancy in percentage of DC white dwarfs between SDSS and our follow-up.

A CMD of the 148 newly observed white dwarfs with discernible spectral types is shown in Figure 1. As expected, the coolest objects at the lower-right-hand region of the CMD are DC white dwarfs. Many of the DAH white dwarfs fall in the massive regions of the CMD, as expected (e.g., [Kawka 2020](#)). The full list of newly observed white dwarf spectral types can be found in Table B1.

2.4. Spectroscopic Observations from the Literature

To compliment our new spectroscopic observations from LDT and SOAR, we also take spectral types and atmospheric parameters from the literature. We find 261 white dwarfs with previously published spectral types, and 161 which have accompanying atmospheric parameters from fitting their spectra¹. The previously published spectral types and atmospheric parameters used in this work can be found in Table C2 along with the relevant references.

The previously published atmospheric parameters compiled in this work come from a variety of sources

that use different sets of spectral models; mainly from [Koester \(2010\)](#) and [Tremblay et al. \(2011\)](#). There could be systematic effects introduced into our results based on two different sets of models and fitting procedures. However, we find no discernible systematic when comparing the two subsets of white dwarf atmospheric parameters determined through the two different models to photometric parameters as discussed in Section 4.1, and do not believe the atmospheric parameters from disparate sources systematically affect our results.

We also cross-match all white dwarfs in wide WD+WD binaries with newly determined spectral types from [Vincent et al. \(2024\)](#), whose spectral typing is determined through a neural-network-based pipeline to select white dwarf candidates and classify their Gaia XP spectra. The pipeline is trained on previously labeled white dwarf spectra from SDSS DR16 ([Ahumada et al. 2020](#)) and achieves an accuracy greater than 90%. We find 1525 white dwarfs that have spectral types determined in this way, with 1292 high-confidence determinations ($P > 0.65$). We only use the high-confidence determinations in this work.

We test the spectral types determined from the Gaia XP spectra by comparing the spectral types from [Vincent et al. \(2024\)](#) to the spectral types gathered in this work from the literature and our follow-up spectra. This consists of 322 individual white dwarfs with high-confidence determinations from [Vincent et al. \(2024\)](#). We find that 8.7% of the spectral types disagree between the Gaia XP determinations and the higher-resolution determinations. This percentage ignores complex spectral type determinations which were not considered in [Vincent et al. \(2024\)](#) (e.g. DAH, DBA, DAZ, etc.). The majority of the disagreements ($\approx 70\%$) come from the higher-resolution spectrum being labelled as a DC while the Gaia XP spectra claim a different spectral type (e.g. DA, DB, or DQ). In our analysis, we ignore the spectral type from the Gaia XP spectra when another spectral type has been determined from higher-resolution spectra.

3. WHITE DWARF AGE DETERMINATIONS

We measure the total ages of the white dwarfs in our sample from both photometric and spectroscopic determinations of their atmospheric parameters.

We take photometric ages from [Heintz et al. \(2022\)](#), which were determined from fits to their spectral energy distributions (SEDs), and assumed a DA spectral type for all white dwarfs in the sample. In brief, a Markov chain Monte Carlo (MCMC) approach is used to fit synthetic fluxes calculated from model DA spectra from [Koester \(2010\)](#) to the observed fluxes in all-sky sur-

¹ We have not included spectral types from the recent result exploring the IFMR by [Hollands et al. \(2024\)](#), but note that 40 of their objects are represented in our new LDT and SOAR data; see Section 3.1.

veys including Gaia, SDSS, the Panoramic Survey Telescope and Rapid Response System (Pan-STARRS), the SkyMapper Southern Sky Survey (SkyMapper), and the Two Micron All-Sky Survey (2MASS). The weighted-mean parallax of the binary is used to get more precise determinations of the components' atmospheric parameters and subsequent total ages, often improving on the mass uncertainties determined from Gaia photometric fitting by Gentile Fusillo et al. (2021).

The spectroscopic ages in this work are derived from atmospheric parameters fit to DA spectra from LDT and SOAR, supplemented by literature determinations. Literature values come from a variety of sources (see Table C2), with some atmospheric parameters determined before 3-D corrections to convective-atmosphere fits were readily available (usually $< 15,000$ K for DAs). We apply 3-D corrections from Tremblay et al. (2013) to the effective temperatures and surface gravities for all DA white dwarfs that have not been previously corrected.

3.1. Spectral Fitting Methods

We determine spectroscopic atmospheric parameters for only the DA white dwarfs in our newly observed sample. To determine the ages of these DA white dwarfs, we first estimate their effective temperatures and surface gravities by fitting their Balmer absorption lines using DA models from Tremblay et al. (2011), with 3-D corrections from Tremblay et al. (2013). The fitting procedure we employ has been outlined in previous works (e.g., Gianninas et al. 2011, Tremblay et al. 2020). The individual Balmer lines are normalized to a continuum determined by fitting a full model spectrum to the observations with a polynomial with 10 free parameters. Then, a χ^2 minimization is performed between the observed and model line profiles, convolved with the instrumental resolution. In this work, we conduct this minimization on the lines H β through H9. This process produces hot and cold solutions on either side of the Balmer maximum ($\approx 13,000$ K). We choose the solution with the closest effective temperature to the photometrically determined atmospheric parameters. We impose a minimum uncertainty of 1.2% on temperature and 0.038 dex on the surface gravity to account for any systematics in the flux calibration and fitting procedure (Liebert et al. 2005). The corresponding fitted temperatures and surface gravities can be found in Table B1.

To validate our spectroscopic fits to the newly observed DAs, we compare derived temperatures and surface gravities from an overlapping sample of 40 white dwarfs observed in common with Hollands et al. (2024), who used spectroscopic observations of wide WD+WD

binaries to constrain the IFMR. Hollands et al. (2024) use a different approach to derive the temperatures and surface gravities as compared to our work: they simultaneously fit the photometry and spectroscopy of both white dwarfs in the binary. We do not find any significant differences between our derived parameters and those derived in Hollands et al. (2024); their effective temperatures are on average 2% cooler, with a standard deviation of 15% about that value, and their surface gravities are on average 0.004 dex smaller (below our imposed minimum uncertainty), with a standard deviation of 0.02 dex about that value. We do not include their atmospheric parameters since they simultaneously include both photometric and spectroscopic information in the fitting procedure.

In rare cases, our independent fitting procedures reveal possible constraints on system histories and architectures. Gaia DR3 4311973098757316608 (WDJ185400.72+104854.69) shows a significant discrepancy between photometric and spectroscopic atmospheric parameters ($\Delta T_{\text{eff}} = 2100$ K and $\Delta \log g = 0.4$ dex). The low photometric surface gravity (7.64 dex) and large temperature discrepancy ($T_{\text{phot}} = 9100$ K; $T_{\text{spec}} = 11,200$ K) suggest Gaia DR3 4311973098757316608 could be a double-degenerate binary and the system is, in fact, a hierarchical triple. The low photometric surface gravity from the source being overluminous in the Gaia CMD suggests that the photometry is blended by a nearby star. This is also supported by the photometric temperature being less than the spectroscopic temperature where the photometric temperature has been influenced by a cooler, fainter companion. Additionally, Gaia DR3 6642323156995855232 (WDJ194406.24-534220.66) and Gaia DR3 4855870439806768512 (WDJ035012.13-383057.28) both show broad line cores which could be indicative of the presence of a modest magnetic field (e.g., Koester et al. 1998). We remove all three objects from future analysis as a result; the corresponding fits can be seen in Figure B8.

3.2. White Dwarf Age Determinations

To derive a total age of a white dwarf, a cooling age and progenitor lifetime must be determined. To derive cooling ages and masses from the spectroscopic temperatures and surface gravities of the DAs in our sample, we use the thick H-layer DA cooling sequences from Bédard et al. (2020).

To determine the progenitor ZAMS lifetimes of the white dwarfs in our sample, we use a theoretically motivated IFMR to connect the initial ZAMS mass of a star to its final white dwarf mass. We use the IFMR

described in Heintz et al. (2022), which uses a theoretical IFMR from Fields et al. (2016) with an offset that is fit using white dwarfs in solar-metallicity clusters (Catalán et al. 2008; Cummings et al. 2015, 2016) and zero-rotation, solar-metallicity stellar models from Modules for Experiments in Stellar Astrophysics (MESA, Paxton et al. 2011, Paxton et al. 2013, Paxton et al. 2015).

In all cases, the dominant contribution to our measured uncertainty on the total white dwarf age hinges on the precision of the white dwarf mass (e.g., Hansen et al. 2004; Kalirai 2012).

4. AGE COMPARISONS AND RESULTS

4.1. Spectroscopic vs. Photometric Parameters

To assess the total ages derived from spectroscopy, we first compare in Figure 2 the derived white dwarf atmospheric parameters to those determined from photometry by Heintz et al. (2022), which utilized the DA white dwarf model atmospheres of Koester (2010). For our spectroscopic fits we use the DA model atmospheres of Tremblay et al. (2011) (see Section 3.1).

Comparing the atmospheric parameters derived from spectroscopy and photometry, we find the effective temperatures derived from both methods are consistent; across the entire sample, the photometric temperatures are on average 1% cooler than the spectroscopic temperatures, with a standard deviation of 10%. This systematic shift is comparable to the minimum uncertainty imposed on the spectroscopic effective temperatures, and is encouraging given photometric fits to SEDs are highly sensitive to the effective temperature. In addition, we find the photometric surface gravities in our sample are systematically 0.03 dex smaller than those derived from spectroscopy, with the $\log g$ differences between photometry and spectroscopy having a standard deviation about that value of 0.23 dex (see middle panel of Figure 2). A difference of 0.23 dex results in mass differences of order $0.2M_{\odot}$. This has a drastic effect on the derived progenitor masses, and subsequently the progenitor lifetimes.

To make sure the use of photometric parameters derived from a different set of models from spectroscopy does not change the trends seen in this section, we fit the photometry of a subset of our sample of 1200 individual white dwarfs with the DA models from Tremblay et al. (2011). These fits use the same fitting technique described in Heintz et al. (2022).

We find the atmospheric parameters from Heintz et al. (2022) derived using photometric fits to Koester (2010) models are entirely consistent, within the reported uncertainties, to photometric fits using the Tremblay et al.

(2011) models. We only see notable discrepancies below <5000 K, where opacities likely differ between the models.

The photometric fits from Heintz et al. (2022) use photometry from a variety of all-sky surveys, but not all white dwarfs fit have the same photometric bands available. Bergeron et al. (2019) found that when using the photometric method, SDSS u-band likely yields the most accurate T_{eff} measurements. However, this is still debated in the literature, since SDSS u-band has an ad-hoc atmospheric transmission correction to align it on the AB system (Eisenstein et al. 2006); Gaia space-based photometry may be more accurate (Tremblay et al. 2019; Gentile Fusillo et al. 2019; McCleery et al. 2020).

For white dwarfs with and without SDSS u-band, we find the same median temperature difference between photometry and spectroscopy as above (1%) and conclude that the absence of SDSS u-band in the photometric fits is not significantly biasing the temperatures. We do find that the inclusion of SDSS u-band improves the agreement of surface gravities between spectroscopy and photometry. For the sample of white dwarfs without SDSS u-band, the surface gravities from spectroscopy are 0.06 dex larger on average which could explain the apparent systematic shift of 0.03 dex seen for the full sample. We do not find that the subset of white dwarfs with SDSS u-band measurably changes the conclusions from the total age agreements from photometric fits discussed in Section 4.2.

We also find an apparent systematic trend wherein the lowest surface gravities determined from spectroscopy deviate more strongly from those determined from photometry (see bottom panel of Figure 2). We find that the best explanation is not an actual physical difference in the fits, but rather that the smaller $\log g$ values from spectroscopy are statistical outliers with larger uncertainties than the photometrically determined values, drawn from a population with surface gravities strongly peaked near $\log g=8.0$ (see more detailed discussion and simulations Appendix A). We find the white dwarfs with higher $\log g$ uncertainties from spectroscopy (>0.2 dex) are mostly cool white dwarfs with effective temperatures <8000 K where the Balmer lines are weak. For these lower effective temperatures, the photometric method is better able to constrain the true surface gravity and should be implemented instead.

These temperature and surface gravity differences are explored further based on a total age comparison for our hypothetically coeval population of wide binaries in the following sections.

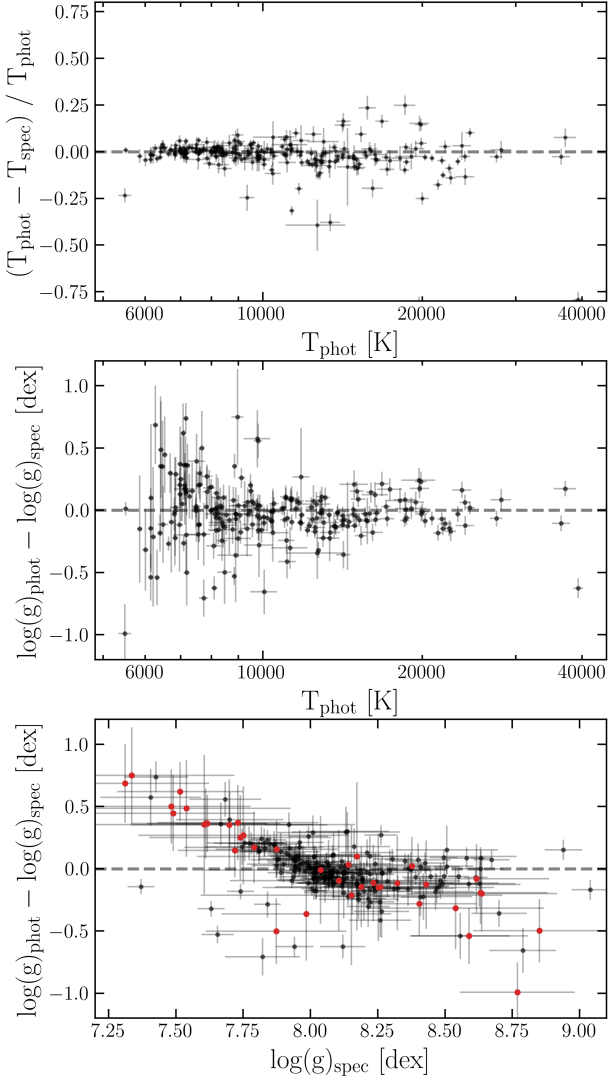


Figure 2. A comparison of derived effective temperatures and surface gravities from photometry and spectroscopy. The top panel shows that the temperature agreement is within 1% across all temperatures. The middle panel shows that there is no trend with surface gravity, and that there is a slight systematic offset of 0.03 dex, where spectroscopy systematically results in slightly more massive solutions. The bottom panel compares photometric and spectroscopic surface gravities, and shows an interesting trend discussed more at length in Appendix A that arises simply from a sample strongly peaked at $\log g=8.0$ with larger uncertainties in spectroscopic fits. The red points in the bottom panel highlight spectroscopic fits with $\log g$ uncertainties > 0.2 dex.

4.2. White Dwarf Age Accuracy and Precision

To assess the accuracy and precision of white dwarf parameters determined from both spectroscopy and photometry, we compare the agreement of the total ages using the parameters from each method.

To start, we look at the sample of white dwarfs with photometric ages that have average total age uncertainties less than 20%, chance alignment factors less than 0.1 (El-Badry et al. 2021), and binary separations greater than 2 arcseconds from Heintz et al. (2022). This results in a subsample of 192 binaries in which these conditions are met for both white dwarfs. In Heintz et al. (2022) a DA atmosphere was assumed for all white dwarfs, and this sample will include DA and non-DA white dwarfs. The 384 white dwarfs in 192 binaries have a mean Gaia G magnitude of 19.2, a mean mass of $0.81 M_{\odot}$, and span the full temperature range of white dwarfs from 4700 K to 30,000 K. The relatively high mean mass is due to the fact that low-mass white dwarfs have larger uncertainties on their progenitor lifetimes and are preferentially removed by the restriction on total age uncertainties. The mean Gaia G magnitude is slightly brighter than the mean magnitude of the full wide WD+WD sample from Heintz et al. (2022) (19.5 mag). When comparing the photometric ages of the two components of the binary, we find good agreement. We find that 58% of the sample has total ages that agree within 28.3% (20% added in quadrature to reflect, at most, 20% total age uncertainties for each white dwarf) of the system’s weighted average age. The median absolute total age difference ($\Delta\tau$) is 0.6 Gyr (or 27% of the system’s average total age). Another way to quantify the agreement between the total ages in each binary is to look at the uncertainties ($\sigma_{\Delta\tau}$) on the total age differences of each system and quote the median $\sigma_{\Delta\tau}$ of the sample. When looking at the uncertainties on the total ages, we find average agreement within 2.2σ . It was found in Heintz et al. (2022) that for more massive white dwarfs ($> 0.67 M_{\odot}$), the reported uncertainties were too small to account for total age differences between the components in wide WD+WD binaries. If we use the recommended inflation factors for the uncertainties, we find average age agreement within 1.4σ .

To compare to the accuracy of white dwarf ages from spectroscopy, we use the sample of 70 DA+DA systems with atmospheric parameters from spectroscopic fits. We perform the same cuts on average total age uncertainties, chance alignment factors, and binary separations, which produce a sample of 14 DA+DA systems with $<20\%$ spectroscopic total age uncertainty on each component. These systems are comparatively much brighter, with a mean Gaia G magnitude of 17.5 (and mean spectroscopic S/N = 35). The mean mass of $0.85 M_{\odot}$ is similar to that of the sample of precise photometric ages discussed above, and temperatures span a large range from 6500 K to 28,000 K. Of these 14 systems, seven (50%) have total age agreement within

28.3% of the weighted average system age. The median $\Delta\tau$ is 0.3 Gyr (or 28% of the system's average age). In terms of $\sigma_{\Delta\tau}$, the average agreement is within 2.1σ . If we apply the same inflation factors that were determined for photometric ages, this agreement improves to 1.5σ . Among this same sample of systems we compare photometrically determined total ages: eight out of 14 systems (57%) have total age agreement within 28.3% of the average age. The average agreement in measured uncertainty is 1.2σ , and improves to 0.6σ on average when inflation factors are applied. The photometric total ages of stars in this sample do not necessarily have $<20\%$ total age uncertainty, which is responsible for the increased level of $\sigma_{\Delta\tau}$ agreement. The sample size of 14 is small, which makes it easy for statistical outliers to affect our conclusions. An increase in the number of systems with high-resolution and high-S/N spectra will help provide stronger conclusions in the future. Since this sample is small, we tabulate these systems in Table 1.

One might expect the spectroscopic method to provide better age constraints for hotter DA white dwarfs, since cooler DAs show weaker lines and thus, may provide less reliable constraints on the atmospheric parameters. Due to the small sample size, we are unable to split the sample into two statistically significant temperature regimes of cool ($<10,000$ K) and hot/warm ($>10,000$ K) but when doing so, we find that the four systems with two cool white dwarfs show stronger total age agreement than the nine systems with two hot white dwarfs.

We conduct a similar investigation into any temperature dependence on our conclusions for the photometric sample. We find that the systems with two cool ($<10,000$ K) white dwarfs show similar total age agreement to systems with two hot/warm ($>10,000$ K) white dwarfs (in both cases, 71% agreeing within 28.3% of the system's average age). However, we find that systems with one cool white dwarf and one hot/warm white dwarf show abnormally high disagreements, with only 12% agreeing within 28.3% of the system's average age. The cause of this discrepancy is unclear.

To understand if an identification spectrum ensures a more accurate total age we use photometric total ages of a sample of 295 DA+DA systems, including ones identified in [Vincent et al. \(2024\)](#) through their Gaia XP spectra. Out of the 295 DA+DA systems, 52 have average photometric total age uncertainties less than 20%, chance alignment factors less than 0.1, and separations greater than 2 arcseconds. This sample of DA+DA binaries is slightly brighter than the photometric sample

discussed previously, with a mean Gaia G magnitude of 18.5. Of these 52 systems, 35 (67%) have total ages that agree within 28.3%. The median $\Delta\tau$ is 0.2 Gyr (or 14% of the system's average age). Incorporating their uncertainties, they agree within 1.9σ on average without inflated errors and 1.0σ with inflated errors. Thus, we find discernible improvement in the accuracy of white dwarf ages when the sample is cleaned of non-DA white dwarfs, demonstrating that collecting an identification spectrum is a crucial step for determining the best ages of an ensemble of white dwarfs. A summary of the level of total age agreement for each sub-sample can be found in Table 2.

It is important to understand when spectroscopy is needed for accurate and precise white dwarf ages. Photometry is readily available for hundreds of thousands of white dwarfs, while spectroscopy can be observationally expensive. From our investigation across the multiple subsets discussed, we find no discernible improvement in age agreement between white dwarfs in wide binaries when spectroscopic fits to Balmer lines are used. Instead, we find that photometric determinations of white dwarf total ages perform better when an identification spectrum is provided and the proper atmospheric models are applied. For spectroscopically identified DA white dwarfs, photometrically determined atmospheric parameters give slightly better total age agreement than spectroscopic fits to the Balmer lines. The sample size of precise spectroscopic total ages is small (14), which makes these conclusions very preliminary. It is important to caveat that this is valid for our spectroscopic S/N; higher S/N and higher-resolution spectra may provide more accurate age constraints.

4.3. Inconsistencies with the Monotonic IFMR

As compared to previous work, many systems in the wide WD+WD binary sample appear to be in contention with our understanding of the IFMR. In [Heintz et al. \(2022\)](#), we found that 21–36% of the systems had a more massive white dwarf with a shorter cooling age. This would imply that the more massive white dwarf had a longer progenitor lifetime and, thus, came from a less massive progenitor. This contradicts the generally accepted monotonic form of the IFMR (e.g., [Cummings et al. 2018](#), [El-Badry et al. 2018](#)), but there has been evidence of a non-monotonic form of the IFMR over a narrow mass range ([Marigo et al. 2020](#)).

We investigate whether such a trend still exists with the addition of spectroscopic information. We take the cooling ages and masses determined in [Heintz et al.](#)

Table 1. Wide WD+WD Binaries Where Both Components are DA and Both Have Precise Spectroscopic Ages

Gaia DR3 source_id1	Gaia DR3 source_id2		T_1 [K]	M_1 [M_\odot]	T_2 [K]	M_2 [M_\odot]	τ_1 [Gyr]	τ_2 [Gyr]
1874954641491354624	1874954645786146304	Phot	18,660 $^{+300}_{-320}$	0.86 $^{+0.01}_{-0.01}$	13,340 $^{+170}_{-160}$	0.75 $^{+0.01}_{-0.01}$	0.45 $^{+0.01}_{-0.01}$	0.78 $^{+0.02}_{-0.02}$
		Spec	19,680 \pm 240	0.89 $^{+0.02}_{-0.02}$	14,400 \pm 440	0.77 $^{+0.02}_{-0.02}$	0.39 $^{+0.02}_{-0.03}$	0.69 $^{+0.04}_{-0.03}$
1911420636118031744	1911420636119326976	Phot	16,320 $^{+350}_{-350}$	0.65 $^{+0.02}_{-0.02}$	13,700 $^{+270}_{-270}$	0.63 $^{+0.02}_{-0.02}$	1.05 $^{+0.36}_{-0.22}$	1.54 $^{+1.13}_{-0.36}$
		Spec	16,960 \pm 200	0.69 $^{+0.02}_{-0.02}$	14,430 \pm 470	0.71 $^{+0.02}_{-0.03}$	0.70 $^{+0.10}_{-0.07}$	0.76 $^{+0.07}_{-0.05}$
2142145385907166208	2142145179748734976	Phot	21,860 $^{+280}_{-300}$	0.68 $^{+0.01}_{-0.01}$	14,900 $^{+180}_{-180}$	0.90 $^{+0.01}_{-0.01}$	0.63 $^{+0.08}_{-0.04}$	0.62 $^{+0.02}_{-0.02}$
		Spec	24,590 \pm 300	0.77 $^{+0.02}_{-0.02}$	16,070 \pm 290	0.98 $^{+0.02}_{-0.02}$	0.38 $^{+0.03}_{-0.03}$	0.55 $^{+0.03}_{-0.03}$
2359214952893455872	2359214952893456000	Phot	12,550 $^{+560}_{-600}$	0.82 $^{+0.03}_{-0.03}$	9560 $^{+410}_{-430}$	0.60 $^{+0.06}_{-0.06}$	0.85 $^{+0.05}_{-0.04}$	6.45 $^{+37.47}_{-4.97}$
		Spec	13,320 \pm 220	0.90 $^{+0.03}_{-0.02}$	10,110 \pm 120	0.67 $^{+0.02}_{-0.03}$	0.79 $^{+0.03}_{-0.03}$	1.36 $^{+0.31}_{-0.09}$
2773334982315549824	2773334978019335040	Phot	22,080 $^{+560}_{-570}$	0.64 $^{+0.02}_{-0.02}$	9820 $^{+150}_{-150}$	0.69 $^{+0.02}_{-0.02}$	1.25 $^{+1.46}_{-0.39}$	1.34 $^{+0.12}_{-0.08}$
		Spec	21,470 \pm 440	0.69 $^{+0.02}_{-0.02}$	10,160 \pm 160	0.79 $^{+0.04}_{-0.04}$	0.59 $^{+0.10}_{-0.08}$	1.28 $^{+0.08}_{-0.06}$
282878984339974528	282878984339976320	Phot	14,150 $^{+500}_{-580}$	0.72 $^{+0.03}_{-0.03}$	12,460 $^{+440}_{-510}$	0.91 $^{+0.03}_{-0.03}$	0.75 $^{+0.10}_{-0.06}$	0.90 $^{+0.06}_{-0.04}$
		Spec	12,140 \pm 240	0.74 $^{+0.04}_{-0.04}$	11,300 \pm 330	0.85 $^{+0.08}_{-0.08}$	0.92 $^{+0.06}_{-0.04}$	1.09 $^{+0.13}_{-0.07}$
3072961070640767488	3072961074934467200	Phot	24,100 $^{+980}_{-1000}$	0.85 $^{+0.03}_{-0.03}$	28,200 $^{+1300}_{-1400}$	1.04 $^{+0.03}_{-0.03}$	0.33 $^{+0.03}_{-0.04}$	0.17 $^{+0.02}_{-0.01}$
		Spec	27,310 \pm 450	0.93 $^{+0.04}_{-0.03}$	27,860 \pm 490	0.98 $^{+0.04}_{-0.04}$	0.20 $^{+0.05}_{-0.02}$	0.18 $^{+0.01}_{-0.01}$
3330855616042214912	3330855616042218112	Phot	18,540 $^{+870}_{-1000}$	1.06 $^{+0.03}_{-0.03}$	15,140 $^{+480}_{-500}$	0.98 $^{+0.02}_{-0.02}$	0.45 $^{+0.02}_{-0.02}$	0.62 $^{+0.02}_{-0.02}$
		Spec	13,930 \pm 440	1.00 $^{+0.02}_{-0.02}$	16,400 \pm 360	0.92 $^{+0.03}_{-0.03}$	0.81 $^{+0.08}_{-0.06}$	0.52 $^{+0.03}_{-0.03}$
5281331588075295232	5281331583776780416	Phot	8260 $^{+370}_{-410}$	0.79 $^{+0.06}_{-0.06}$	8390 $^{+480}_{-550}$	0.84 $^{+0.08}_{-0.08}$	2.02 $^{+0.15}_{-0.20}$	2.25 $^{+0.27}_{-0.25}$
		Spec	8830 \pm 110	0.89 $^{+0.04}_{-0.04}$	8560 \pm 100	0.90 $^{+0.05}_{-0.05}$	2.28 $^{+0.26}_{-0.27}$	2.55 $^{+0.28}_{-0.35}$
5490676742283052800	5490676707920375936	Phot	8980 $^{+520}_{-570}$	0.71 $^{+0.09}_{-0.08}$	10,460 $^{+880}_{-1010}$	1.00 $^{+0.10}_{-0.08}$	1.53 $^{+0.98}_{-0.16}$	1.82 $^{+0.16}_{-0.09}$
		Spec	9060 \pm 110	0.85 $^{+0.05}_{-0.05}$	9640 \pm 120	1.00 $^{+0.05}_{-0.05}$	1.87 $^{+0.28}_{-0.20}$	2.32 $^{+0.26}_{-0.29}$
5564028981196462336	5564029702750970112	Phot	7090 $^{+90}_{-90}$	0.59 $^{+0.01}_{-0.01}$	6150 $^{+70}_{-70}$	0.60 $^{+0.01}_{-0.01}$	11.43 $^{+1.74}_{-1.44}$	8.71 $^{+1.93}_{-1.31}$
		Spec	7220 \pm 90	0.75 $^{+0.03}_{-0.04}$	6400 \pm 110	0.94 $^{+0.11}_{-0.12}$	2.73 $^{+0.33}_{-0.26}$	5.22 $^{+0.32}_{-0.64}$
5780478664144123264	5780478664144129152	Phot	9380 $^{+230}_{-240}$	0.66 $^{+0.03}_{-0.04}$	9000 $^{+260}_{-260}$	0.77 $^{+0.04}_{-0.04}$	1.64 $^{+1.19}_{-0.26}$	1.59 $^{+0.07}_{-0.06}$
		Spec	9350 \pm 110	0.67 $^{+0.02}_{-0.02}$	8520 \pm 100	0.75 $^{+0.04}_{-0.04}$	1.52 $^{+0.23}_{-0.07}$	1.77 $^{+0.09}_{-0.06}$
630770819920096640	630770819920096768	Phot	24,080 $^{+570}_{-590}$	0.88 $^{+0.02}_{-0.02}$	22,620 $^{+550}_{-610}$	1.14 $^{+0.01}_{-0.01}$	0.31 $^{+0.02}_{-0.03}$	0.34 $^{+0.01}_{-0.01}$
		Spec	24,670 \pm 390	0.84 $^{+0.03}_{-0.03}$	25,780 \pm 590	1.21 $^{+0.03}_{-0.03}$	0.33 $^{+0.02}_{-0.02}$	0.32 $^{+0.04}_{-0.03}$
6898489884295412352	6898489884295407488	Phot	10,870 $^{+130}_{-130}$	0.87 $^{+0.01}_{-0.01}$	8230 $^{+100}_{-100}$	0.71 $^{+0.01}_{-0.01}$	1.20 $^{+0.02}_{-0.02}$	1.82 $^{+0.06}_{-0.04}$
		Spec	10,580 \pm 130	0.86 $^{+0.02}_{-0.02}$	8140 \pm 100	0.72 $^{+0.05}_{-0.05}$	1.26 $^{+0.05}_{-0.05}$	1.95 $^{+0.20}_{-0.08}$

Table 2. Age Agreement for Different Samples of Wide WD+WD Binaries

Sample	N	$\Delta\tau < 28.3\% \tau_{avg}$	Median $\Delta\tau$ (Gyr, % of τ_{avg})	Median σ	Median $\sigma_{inflated}$
			Agreement	Agreement	
Phot Ages with $\sigma_\tau < 20\%$	192	58%	0.6 (23%)	2.2	1.4
Spec Ages with $\sigma_\tau < 20\%$	14	50%	0.3 (28%)	2.1	1.5
Phot Ages with ID Spectrum and $\sigma_\tau < 20\%$	52	67%	0.2 (14%)	1.9	1.0

NOTE— τ_{avg} refers to the weighted average age of the binary and $\sigma_{inflated}$ references the total age agreement when inflation factors from Heintz et al. (2022) are applied to the total age uncertainties.

(2022), which assumed a DA atmosphere for all white dwarfs, in conjunction with the spectral types gathered in this work. We find 34% of the DA+DA systems are in contention with a monotonic IFMR, while 18% are more than 1σ away from being consistent with the monotonic IFMR (see top left panel of Figure 3). In addition, we find that DA+non-DA systems show 66% of the systems are inconsistent with a monotonic IFMR while 51% show inconsistencies that are greater than 1σ . For non-DA+non-DA systems, we find 71% of the systems are inconsistent with 43% having inconsistencies greater than 1σ .

The larger number of inconsistent systems among those with a non-DA component could result from incorrect atmospheres being applied to their photometry. Fitting a DA model to a non-DA can introduce systematic errors on the order of 10–15% on WD mass (Giannicchele et al. 2012). To alleviate this problem, we conduct SED fits to all the spectroscopically confirmed DB and DC white dwarfs using the appropriate atmospheric models. We perform the same fitting methods and quality control checks outlined in Heintz et al. (2022) (see summary in Section 4.1).

For DB white dwarfs, we use the pure helium-atmosphere models from Cukanovaite et al. (2021) and the thin H-layer cooling models from Bédard et al. (2020). For the DC white dwarfs in the sample, we follow Vincent et al. 2024: For DCs with $T_{\text{eff}} < 5500$ K, we use the DA fits done previously in Heintz et al. (2022). For DCs with $5500 < T_{\text{eff}} < 11,000$ K, we use mixed-atmosphere models with H/He ratios of 10^{-5} from Cukanovaite et al. (2021) and the corresponding thin H-layer cooling models from Bédard et al. (2020). For DCs with $T_{\text{eff}} > 11,000$ K, we use the same pure He models used in the DB fits.

Figure 3 shows the distribution of the binaries’ mass difference and cooling age difference when using the correct models. We see significant improvement in the number of inconsistent systems for the DB white dwarfs, but 42% are still inconsistent with a monotonically increasing IFMR, with 16% being more than 1σ inconsistent. Most of the IFMRs to date have been constrained only with DA white dwarfs and an IFMR for DB white dwarfs remains elusive (Barnett et al. 2021).

The number of systems with a DB white dwarf that are inconsistent with the monotonic IFMR is in line with the fraction of known DA+DA systems with inconsistent cooling ages and masses. This leaves two possibilities: either roughly 20% of wide WD+WD binaries suffer from merger contamination or blended photometry and were likely born as triple systems, or the IFMR is not monotonic. We do not find that white dwarfs in in-

consistent systems are preferentially found at any mass range when compared to the full sample. 58% of binaries in the DA+DA sample shown in Figure 3 that are inconsistent with a monotonic IFMR have at least one white dwarf with a mass between $0.6 M_{\odot}$ and $0.7 M_{\odot}$. This is not surprising given that the white dwarf mass distribution peaks in this range (Tremblay et al. 2019).

For systems with at least one DC white dwarf, we find that the inconsistency reaches 40% even using non-DA atmospheres (see bottom panels of Figure 3). We suspect this reflects the inaccuracy of photometrically determined parameters for DC white dwarfs due to the inexact understanding of their atmospheric compositions, although it may also point to a higher fraction of merger contaminants among DC white dwarfs. While it has been widely thought that hotter DCs ($> 11,000$ K) are strongly magnetic and a signpost of a past merger (e.g., Briggs et al. 2015), we find that cooler DCs in our sample still show significant disagreement (59% of the 62 DA+DC and DC+DC systems with DC temperatures $< 11,000$ K are inconsistent with a monotonically increasing IFMR).

To determine if the percentages of inconsistent systems we find are not due to random errors, we generate a mock sample of 5000 binaries with masses in the range of $1 - 8 M_{\odot}$ determined through a Salpeter initial-mass function (IMF, Salpeter 1955). We set the criteria that their total ages must be the same and use the IFMR discussed in Section 3.2 to convert the ZAMS mass to the final white dwarf mass. The cooling age is determined by subtracting the progenitor lifetime for the given ZAMS mass (determined through the MESA evolutionary sequences discussed in Section 3.2). Then, the white dwarf cooling age and mass are converted into the white dwarf’s temperature using the cooling models from Bédard et al. (2020). We introduce random errors into the white dwarf mass and temperatures which are drawn from the distribution of reported uncertainties on temperature and mass from the photometric fits conducted in Heintz et al. (2022). Finally, we count the number of systems in contention with the monotonic IFMR. We find that for the sample of 5000 binaries, 18% are inconsistent with a monotonic IFMR simply due to random errors with only 1.3% of those systems being more than 1σ away from being consistent. To better represent the sample size of the DA+DA binaries in our sample, we conduct the same test 20 times with 100 binaries. Through this test, we find $19^{+4}_{-5}\%$ to be inconsistent with the monotonic IFMR with only $1.5 \pm 1.5\%$ are more than 1σ away from the being consistent.

For the DA+DA and DA+DB binaries, we find 20% of the systems are more than 1σ inconsistent with a

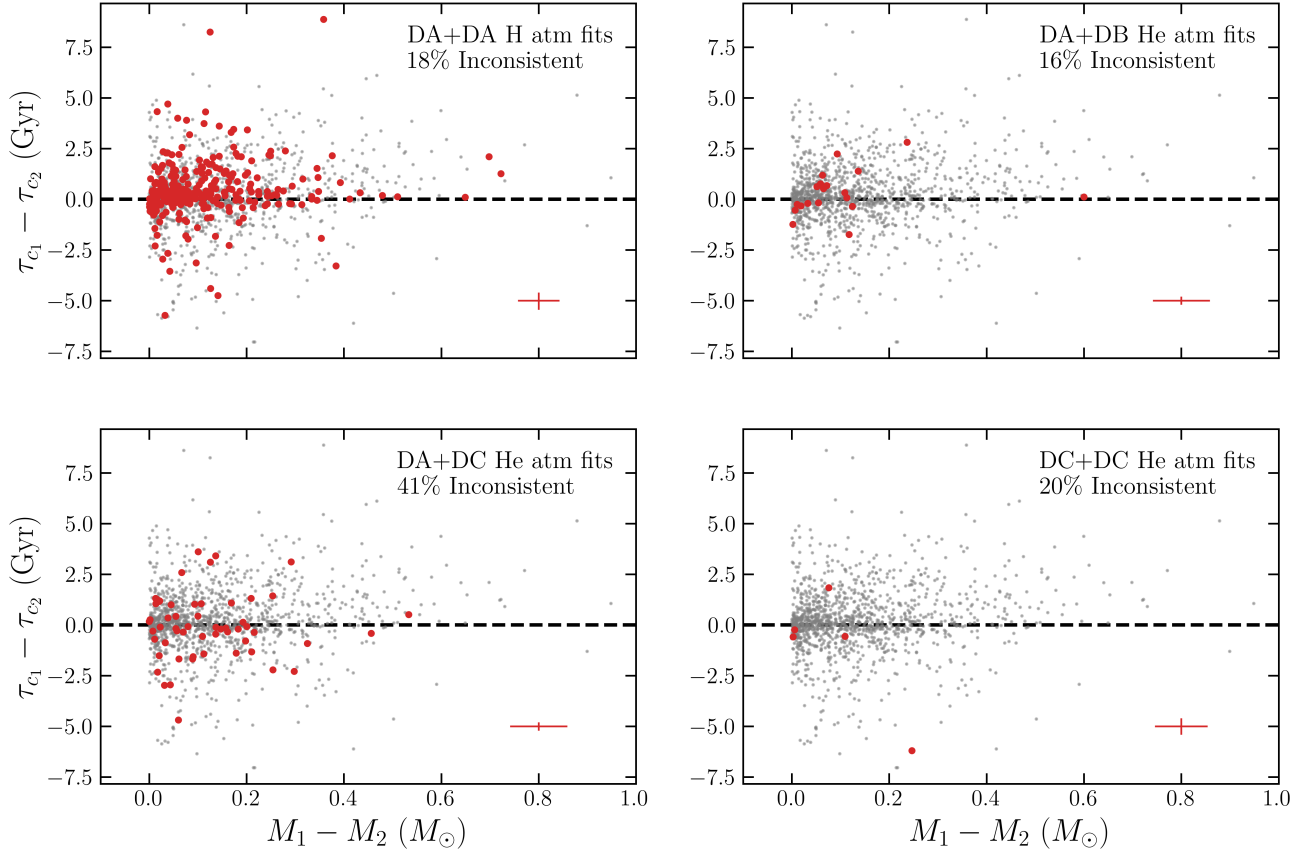


Figure 3. Comparison of cooling age difference versus mass difference using the correct model atmospheres for photometric fitting (red points). The grey points in each panel are from all WD+WD binaries in Heintz et al. (2022). The percentage of systems in contention with the monotonic IFMR are shown in each panel as well. The number of systems in contention with a monotonic IFMR are determined as the number of systems more than 1σ away from having $\tau_{c1} > \tau_{c2}$.

An average uncertainty is shown in the bottom right of each panel. Using the correct atmospheric parameters for DA+DB systems produces a roughly similar number of ill-behaved systems as the known DA+DA systems; a larger number of systems with at least one DC appear in contention with the monotonic IFMR.

monotonic IFMR. The number of systems more than 1σ away from being consistent is minimally affected by random statistical errors, and thus, we conclude that the number of systems inconsistent with a monotonic IFMR is roughly 20% for the DA+DA and DA+DB binaries.

4.4. Other White Dwarf Spectral Types

Using our follow-up observations and collected literature spectra we identified several components of wide WD+WD systems that are noteworthy, including systems with metal-polluted white dwarfs (DZ), white dwarfs with carbon features in their spectra (DQ), and highly magnetic white dwarfs (DAH) (see Section 2.3).

4.4.1. Metal-Polluted Systems

Metal pollution can provide insights into the remnants of planetary systems around white dwarfs. In our follow-up work, we discover a new DZ+DA binary system. The primary (Gaia DR3 4471738941493617408, WDJ181332.20+060412.61) is a $0.66 M_\odot$ DZ white

dwarf at 7600 K, and the secondary (Gaia DR3 4471739010213094272, WDJ181330.47+060412.51) is a 6500 K, $0.62 M_\odot$ DA white dwarf. The mean weighted age of the system is 2.3 ± 0.2 Gyr, and the total age difference between the two stars is $1.9^{+3.2}_{-0.9}$ Gyr. Systems like this provide a great opportunity to test DZ atmospheric models against their DA counterparts.

We identify a total of 22 wide WD+WD systems with at least one DZ. Of these 22 systems, 17 are identified through their Gaia XP spectra alone (Vincent et al. 2024). For these DZ white dwarfs, we employ the same criteria used for DC white dwarfs to determine their atmospheric parameters from photometry (see Section 4.3). If the white dwarf has observable H (DAZ) or He (DBZ) lines, we use the appropriate pure H and He models, respectively. Of the 22 systems containing a metal-polluted white dwarf, 13 suggest the more massive white dwarf has a shorter cooling age. This level of inconsistency for the DZ white dwarfs parallels the DC white

dwarf population. This adds more evidence that the problem with the DC white dwarfs is an improper application of mixed- and He-atmosphere models and not an intrinsically higher number of mergers among their population, although it is possible that a large fraction of the 17 identified by their Gaia XP spectra could be improperly labelled as DZ white dwarfs.

4.4.2. Magnetic White Dwarfs

We identify 16 wide WD+WD systems with at least one DAH white dwarf. [Vincent et al. \(2024\)](#) do not make attempts to identify and classify magnetic white dwarfs through Gaia XP spectra. Thus, all magnetic white dwarfs in the sample are manually classified from their spectra.

From our follow-up observations, we identify 3 new DA+DAH systems and one new DAH+DAH system. The first system contains a 10,500 K, $0.86 M_{\odot}$ DAH primary (Gaia DR3 4940155500795290624, WDJ022440.28-461133.91) with an 11,700 K, $0.71 M_{\odot}$ DA secondary (Gaia DR3 4940155500795290880, WDJ022440.65-461140.65). The second system contains an 8100 K, $0.88 M_{\odot}$ DA primary (Gaia DR3 5062948237833763840, WDJ024051.59-324837.30) with a 7500 K, $0.79 M_{\odot}$ DAH secondary (Gaia DR3 5062948340912201088, WDJ024051.94-324814.09). The last DA+DAH system contains a 9700 K, $1.02 M_{\odot}$ DAH primary (Gaia DR3 6093462311215003776, WDJ135006.24-502534.22) and a 6500 K, $0.66 M_{\odot}$ DA secondary (Gaia DR3 6093462315507278208, WDJ135006.04-502540.07). The new DAH+DAH system contains a 14,000 K, $1.09 M_{\odot}$ DAH primary (Gaia DR3 5551794951535528448, WDJ064715.56-470733.36) with an 11,500 K, $0.99 M_{\odot}$ DAH secondary (Gaia DR3 5551794951535526144, WDJ064716.66-470744.24).

Of the 16 systems with at least one DAH, four have a more massive white dwarf with a shorter cooling age. The percentage of inconsistent systems is comparable to the sample of DA+DA systems. This indicates that the merger fraction among magnetic white dwarfs is not noticeably higher in our sample, which is not surprising given 11 of the 16 DAHs are cooler than 10,000 K. These cooler magnetic white dwarfs are generally not massive and do not require dynamo generation from a merger, supporting similar conclusions from field white dwarfs within 40 pc by [Bagnulo & Landstreet \(2022\)](#). When labelling hot DCs ($> 11,000$ K) as magnetic white dwarfs and using H atmosphere fits, we find the magnetic white dwarfs do have higher inconsistencies with the monotonic IFMR (52% inconsistent with 39% more than 1σ inconsistent). The implication is that these hot DCs may have H or He lines, but very strong (often

>100 MG) magnetic fields have shifted these absorption lines all over the spectrum (e.g., [Caiazzo et al. 2021](#)). With the inclusion of hot DCs, we find that the most strongly magnetic white dwarfs are ill-behaved, in line with the idea that strong magnetism is a signpost for mergers (e.g., [Kilic et al. 2023](#)).

4.4.3. DQ White Dwarfs

Hot ($>15,000$ K) and warm ($10,000 < T_{\text{eff}} < 15,000$ K) DQ white dwarfs are hypothesized to form in binary mergers (e.g., [Dunlap & Clemens 2015](#); [Williams et al. 2016](#); [Kawka et al. 2020](#)). If the DQs in our sample did, in fact, form from a binary interaction, their cooling ages would be inconsistent with an increasing IFMR.

We identify 11 wide WD+WD systems with at least one DQ. Of these 11 systems, 4 are identified from their Gaia XP spectra alone ([Vincent et al. 2024](#)). For atmospheric parameters and cooling ages of the DQs in the sample, we use the He-atmosphere models that we use for the DB and DC white dwarfs described in Section 4.3. Of the 11 systems with a DQ white dwarf component, nine have the more massive white dwarf with a shorter cooling age. Of the nine systems in which the more massive white dwarf has a shorter cooling age, we do not see any preference for higher temperatures with the sample spanning a temperature range of 6700-9500 K. These DQs are not part of the hot/warm population theorized to form from binary mergers and there is no clear evidence of DQs in this temperature range having a higher expected merger fraction (e.g., [Coutu et al. 2019](#); [Koester & Kepler 2019](#)). Improved modeling of this sub-sample could help discern if this inconsistency arises purely from incorrect model atmospheres, or if DQ white dwarfs in this temperature range are preferentially formed in mergers.

5. DISCUSSION AND CONCLUSIONS

In this work, we collected spectral types for 419 individual white dwarfs in wide (separated by >100 au) WD+WD binaries, as well as spectral types of 1292 individual white dwarfs from [Vincent et al. \(2024\)](#), identified from their Gaia XP spectra. We additionally derived atmospheric parameters from spectra for 256 of the 419 white dwarfs, with 94 new atmospheric parameters determined from our spectroscopic follow-up.

The main conclusions of this work can be summarized as follows:

- We find that fits to optical spectra of white dwarfs do not provide any noticeable improvement in agreement between the total ages of white dwarfs in wide WD+WD binaries. 50% of wide WD+WD systems with precise total ages from spectroscopy

($<20\%$ uncertainties) agree within 28.28% (20% added in quadrature) of the weighted mean age of the system. This nearly matches, albeit with slightly worse performance, what is found in photometrically determined ages (57%). The mean magnitude of the sample with $<20\%$ total age uncertainties from spectroscopy is $G = 17.5$ mag, which is much brighter than the sample with $<20\%$ total age uncertainties from photometry (mean of $G = 19.2$ mag), highlighting the capability of photometry combined with Gaia parallaxes to provide precise total ages for fainter objects.

- We find that collecting an identification spectrum is a crucial step in determining the most accurate white dwarf total ages. For a sample of photometric white dwarf total ages spectroscopically identified as DAs, we find that 67% of systems with precise total ages (uncertainties $<20\%$) agree within 28.28% of the weighted mean total age of the system. This noticeably improves on samples of precisely aged systems from photometry when a DA model is assumed for all white dwarfs (57%), and on precisely determined total ages from spectroscopy (50%).
- Roughly 20% of white dwarfs in wide WD+WD binaries are inconsistent with a monotonically increasing IFMR. This discrepancy was first seen in Heintz et al. (2022) and is still present when more spectroscopic information is available, and when the correct atmosphere models are used for SED fits to determine the total age of the white dwarf from mass and effective temperature. This inconsistency is seen in multiple samples of spectroscopically identified wide WD+WD binaries, including DA+DA, DA+DB, DA+DC, and DC+DC. These systems could not have formed through single-star evolution assuming a monotonic IFMR and, thus, could be merger products or contain close binary systems masking as single stars which contaminate the data. Roughly 20% of the sample being merger remnants is consistent with binary population synthesis models (Temmink et al. 2020). The implication that 20% of the wide binary sample started off as triples is not unreasonable given the fraction of white dwarf progenitors that are expected to be born in binaries versus triples (Moe & Di Stefano 2017; Shariat et al. 2023).

This result could also be explained by a non-monotonic IFMR, which has gained support in recent years from white dwarfs with masses between 0.6 - $0.7 M_{\odot}$ (Marigo et al. 2020). We do

not find that white dwarfs in inconsistent systems cluster at any mass range when compared to the full sample. 58% of systems in the DA+DA sample that are inconsistent with a monotonic IFMR have at least one white dwarf with a mass between $0.6 M_{\odot}$ and $0.7 M_{\odot}$, but we expect most to lie in this range given the white dwarf mass distribution peaks here (Tremblay et al. 2019).

- We find that wide binaries containing DC white dwarfs are more often incompatible with a monotonically increasing IFMR than systems containing DA or DB white dwarfs. It is difficult to distinguish whether this effect is due to a larger merger population among DC white dwarfs or the incorrect application of atmospheric models. Because it is challenging to identify the atmospheric compositions of DC white dwarfs in our sample, we imposed criteria (see Section 4.3) dependent on the temperature of the DC. This method likely applies incorrect models to a subset of the DCs, which may contribute to higher inconsistency with the IFMR.

This work provides an empirical demonstration of the strengths and challenges of using white dwarfs as stellar age indicators. We find unavoidable systematic effects from past mergers among white dwarfs, though mergers are not unique to white dwarf stars and provide a challenge for any stellar age indicator. We also find that obtaining identification spectra is a crucial step for determining accurate white dwarf total ages.

The sample of spectroscopically identified white dwarfs in wide binaries will increase significantly with ongoing and upcoming all-sky, multiplexed spectroscopic surveys such as SDSS-V (Almeida et al. 2023) and DESI (Cooper et al. 2023). These surveys will be vital in getting the largest possible sample of spectroscopically identified white dwarfs which in turn will allow for more accurate white dwarf age estimates. As the sample of white dwarfs with optical spectra increases, conclusions from tests of spectroscopic fits to Balmer lines will only strengthen. As of now, with our small sample of precise ages, we find that these spectroscopic fits do not provide more accurate total ages and, in fact, are generally as good as photometric fits to white dwarfs with unidentified spectral types.

6. ACKNOWLEDGEMENTS

We acknowledge helpful comments from the anonymous referee that helped to improve this work. We acknowledge support from the National Science Foundation under Grant No. AST-1908119 as well as under

Grant No. PHY-1748958. PET received funding from the European Research Council under the European Union’s Horizon 2020 research and innovation programme number 101002408 (MOS100PC). JR and BK acknowledge funding from the National Science Foundation under grant number AST-2108311 and from the NC Space Grant Graduate Research Fellowship.

We sincerely thank our excellent telescope operators and support staff Patricio Ugarte, Carlos Corco, Juan Espinoza, Rodrigo Hernández, and Sergio Pizarro from SOAR and Teznie Pugh, Ana Hayslip, LaLaina Shumar, Jason Sanborn, Haylee Archer, Ishara Nisley, Sydney Perez, Ben Shafransky, Jose Fernandez, and Stephen Levine from Lowell Observatory. We also appreciate observing assistance while in training from Ryan Hegedus. These results made use of the Lowell Discovery

Telescope (LDT) at Lowell Observatory. Lowell is a private, non-profit institution dedicated to astrophysical research and public appreciation of astronomy and operates the LDT in partnership with Boston University, the University of Maryland, the University of Toledo, Northern Arizona University and Yale University. The upgrade of the DeVeny optical spectrograph has been funded by a generous grant from John and Ginger Giovale and by a grant from the Mt. Cuba Astronomical Foundation. These results are based in part on observations obtained at the Southern Astrophysical Research (SOAR) telescope, which is a joint project of the Ministério da Ciência, Tecnologia e Inovações (MCTI/LNA) do Brasil, the US National Science Foundation’s NOIRLab, the University of North Carolina at Chapel Hill (UNC), and Michigan State University (MSU).

REFERENCES

- Ahumada, R., Allende Prieto, C., Almeida, A., et al. 2020, ApJS, 249, 3, doi: [10.3847/1538-4365/ab929e](https://doi.org/10.3847/1538-4365/ab929e)
- Almeida, A., Anderson, S. F., Argudo-Fernández, M., et al. 2023, ApJS, 267, 44, doi: [10.3847/1538-4365/acda98](https://doi.org/10.3847/1538-4365/acda98)
- Andrews, J. J., Agüeros, M. A., Gianninas, A., et al. 2015, ApJ, 815, 63, doi: [10.1088/0004-637X/815/1/63](https://doi.org/10.1088/0004-637X/815/1/63)
- Bagnulo, S., & Landstreet, J. D. 2022, ApJL, 935, L12, doi: [10.3847/2041-8213/ac84d3](https://doi.org/10.3847/2041-8213/ac84d3)
- Barnes, S. A. 2007, ApJ, 669, 1167, doi: [10.1086/519295](https://doi.org/10.1086/519295)
- Barnett, J. W., Williams, K. A., Bédard, A., & Bolte, M. 2021, AJ, 162, 162, doi: [10.3847/1538-3881/ac1423](https://doi.org/10.3847/1538-3881/ac1423)
- Barrientos, M., & Chanamé, J. 2021, ApJ, 923, 181, doi: [10.3847/1538-4357/ac2f49](https://doi.org/10.3847/1538-4357/ac2f49)
- Baxter, R. B., Dobbie, P. D., Parker, Q. A., et al. 2014, MNRAS, 440, 3184, doi: [10.1093/mnras/stu464](https://doi.org/10.1093/mnras/stu464)
- Bédard, A., Bergeron, P., Brassard, P., & Fontaine, G. 2020, ApJ, 901, 93, doi: [10.3847/1538-4357/abafbe](https://doi.org/10.3847/1538-4357/abafbe)
- Berger, T. A., Huber, D., Gaidos, E., & van Saders, J. L. 2018, ApJ, 866, 99, doi: [10.3847/1538-4357/aada83](https://doi.org/10.3847/1538-4357/aada83)
- Bergeron, P., Dufour, P., Fontaine, G., et al. 2019, ApJ, 876, 67, doi: [10.3847/1538-4357/ab153a](https://doi.org/10.3847/1538-4357/ab153a)
- Bergeron, P., Wesemael, F., Dufour, P., et al. 2011, ApJ, 737, 28, doi: [10.1088/0004-637X/737/1/28](https://doi.org/10.1088/0004-637X/737/1/28)
- Bida, T. A., Dunham, E. W., Massey, P., & Roe, H. G. 2014, in Society of Photo-Optical Instrumentation Engineers (SPIE) Conference Series, Vol. 9147, Ground-based and Airborne Instrumentation for Astronomy V, ed. S. K. Ramsay, I. S. McLean, & H. Takami, 91472N, doi: [10.1117/12.2056872](https://doi.org/10.1117/12.2056872)
- Briceño, C., Heathcote, S., Cecil, G., et al. 2018, in Society of Photo-Optical Instrumentation Engineers (SPIE) Conference Series, Vol. 10700, Ground-based and Airborne Telescopes VII, ed. H. K. Marshall & J. Spyromilio, 107003Z, doi: [10.1117/12.2314026](https://doi.org/10.1117/12.2314026)
- Briggs, G. P., Ferrario, L., Tout, C. A., Wickramasinghe, D. T., & Hurley, J. R. 2015, MNRAS, 447, 1713, doi: [10.1093/mnras/stu2539](https://doi.org/10.1093/mnras/stu2539)
- Brown, W. R., Geller, M. J., Kenyon, S. J., Kurtz, M. J., & Bromley, B. C. 2007, ApJ, 671, 1708, doi: [10.1086/523642](https://doi.org/10.1086/523642)
- Caiazzo, I., Burdge, K. B., Fuller, J., et al. 2021, Nature, 595, 39, doi: [10.1038/s41586-021-03615-y](https://doi.org/10.1038/s41586-021-03615-y)
- Catalán, S., Isern, J., García-Berro, E., & Ribas, I. 2008, MNRAS, 387, 1693, doi: [10.1111/j.1365-2966.2008.13356.x](https://doi.org/10.1111/j.1365-2966.2008.13356.x)
- Chaplin, W. J., Basu, S., Huber, D., et al. 2014, ApJS, 210, 1, doi: [10.1088/0067-0049/210/1/1](https://doi.org/10.1088/0067-0049/210/1/1)
- Cheng, S., Cummings, J. D., & Ménard, B. 2019, ApJ, 886, 100, doi: [10.3847/1538-4357/ab4989](https://doi.org/10.3847/1538-4357/ab4989)
- Claytor, Z. R., van Saders, J. L., Santos, Á. R. G., et al. 2020, ApJ, 888, 43, doi: [10.3847/1538-4357/ab5c24](https://doi.org/10.3847/1538-4357/ab5c24)
- Clemens, J. C., Crain, J. A., & Anderson, R. 2004, in Society of Photo-Optical Instrumentation Engineers (SPIE) Conference Series, Vol. 5492, Ground-based Instrumentation for Astronomy, ed. A. F. M. Moorwood & M. Iye, 331–340, doi: [10.1117/12.550069](https://doi.org/10.1117/12.550069)
- Cooper, A. P., Koposov, S. E., Allende Prieto, C., et al. 2023, ApJ, 947, 37, doi: [10.3847/1538-4357/acb3c0](https://doi.org/10.3847/1538-4357/acb3c0)
- Coutu, S., Dufour, P., Bergeron, P., et al. 2019, ApJ, 885, 74, doi: [10.3847/1538-4357/ab46b9](https://doi.org/10.3847/1538-4357/ab46b9)

- Croom, S. M., Smith, R. J., Boyle, B. J., et al. 2004, MNRAS, 349, 1397, doi: [10.1111/j.1365-2966.2004.07619.x](https://doi.org/10.1111/j.1365-2966.2004.07619.x)
- Cukanovaite, E., Tremblay, P.-E., Bergeron, P., et al. 2021, MNRAS, 501, 5274, doi: [10.1093/mnras/staa3684](https://doi.org/10.1093/mnras/staa3684)
- Cummings, J. D., & Kalirai, J. S. 2018, AJ, 156, 165, doi: [10.3847/1538-3881/aad5df](https://doi.org/10.3847/1538-3881/aad5df)
- Cummings, J. D., Kalirai, J. S., Choi, J., et al. 2019, ApJL, 871, L18, doi: [10.3847/2041-8213/aafc2d](https://doi.org/10.3847/2041-8213/aafc2d)
- Cummings, J. D., Kalirai, J. S., Tremblay, P. E., & Ramirez-Ruiz, E. 2015, ApJ, 807, 90, doi: [10.1088/0004-637X/807/1/90](https://doi.org/10.1088/0004-637X/807/1/90)
- . 2016, ApJ, 818, 84, doi: [10.3847/0004-637X/818/1/84](https://doi.org/10.3847/0004-637X/818/1/84)
- Cummings, J. D., Kalirai, J. S., Tremblay, P. E., Ramirez-Ruiz, E., & Choi, J. 2018, ApJ, 866, 21, doi: [10.3847/1538-4357/aadfd6](https://doi.org/10.3847/1538-4357/aadfd6)
- Cunningham, T., Tremblay, P.-E., & W. O'Brien, M. 2024, MNRAS, 527, 3602, doi: [10.1093/mnras/stad3275](https://doi.org/10.1093/mnras/stad3275)
- Curtis, J. L., Agüeros, M. A., Matt, S. P., et al. 2020, ApJ, 904, 140, doi: [10.3847/1538-4357/abbf58](https://doi.org/10.3847/1538-4357/abbf58)
- Dobbie, P. D., Baxter, R., Külebi, B., et al. 2012, MNRAS, 421, 202, doi: [10.1111/j.1365-2966.2012.20291.x](https://doi.org/10.1111/j.1365-2966.2012.20291.x)
- Dotter, A. 2016, ApJS, 222, 8, doi: [10.3847/0067-0049/222/1/8](https://doi.org/10.3847/0067-0049/222/1/8)
- Dunlap, B. H., & Clemens, J. C. 2015, in Astronomical Society of the Pacific Conference Series, Vol. 493, 19th European Workshop on White Dwarfs, ed. P. Dufour, P. Bergeron, & G. Fontaine, 547
- Eisenstein, D. J., Liebert, J., Harris, H. C., et al. 2006, ApJS, 167, 40, doi: [10.1086/507110](https://doi.org/10.1086/507110)
- El-Badry, K., & Rix, H.-W. 2018, MNRAS, 480, 4884, doi: [10.1093/mnras/sty2186](https://doi.org/10.1093/mnras/sty2186)
- El-Badry, K., Rix, H.-W., & Heintz, T. M. 2021, MNRAS, doi: [10.1093/mnras/stab323](https://doi.org/10.1093/mnras/stab323)
- El-Badry, K., Rix, H.-W., & Weisz, D. R. 2018, ApJL, 860, L17, doi: [10.3847/2041-8213/aaaca9c](https://doi.org/10.3847/2041-8213/aaaca9c)
- Fields, C. E., Farmer, R., Petermann, I., Iliadis, C., & Timmes, F. X. 2016, ApJ, 823, 46, doi: [10.3847/0004-637X/823/1/46](https://doi.org/10.3847/0004-637X/823/1/46)
- Finley, D. S., & Koester, D. 1997, ApJL, 489, L79, doi: [10.1086/310967](https://doi.org/10.1086/310967)
- Fontaine, G., Brassard, P., & Bergeron, P. 2001, PASP, 113, 409, doi: [10.1086/319535](https://doi.org/10.1086/319535)
- Fouesneau, M., Rix, H.-W., von Hippel, T., Hogg, D. W., & Tian, H. 2019, ApJ, 870, 9, doi: [10.3847/1538-4357/aaeee74](https://doi.org/10.3847/1538-4357/aaeee74)
- Gaia Collaboration, Prusti, T., de Bruijne, J. H. J., et al. 2016, A&A, 595, A1, doi: [10.1051/0004-6361/201629272](https://doi.org/10.1051/0004-6361/201629272)
- Gaia Collaboration, Brown, A. G. A., Vallenari, A., et al. 2018, A&A, 616, A1, doi: [10.1051/0004-6361/201833051](https://doi.org/10.1051/0004-6361/201833051)
- . 2021, A&A, 649, A1, doi: [10.1051/0004-6361/202039657](https://doi.org/10.1051/0004-6361/202039657)
- Gentile Fusillo, N. P., Tremblay, P.-E., Gänsicke, B. T., et al. 2019, MNRAS, 482, 4570, doi: [10.1093/mnras/sty3016](https://doi.org/10.1093/mnras/sty3016)
- Gentile Fusillo, N. P., Tremblay, P. E., Cukanovaite, E., et al. 2021, MNRAS, 508, 3877, doi: [10.1093/mnras/stab2672](https://doi.org/10.1093/mnras/stab2672)
- Giannicche, N., Bergeron, P., & Dufour, P. 2012, ApJS, 199, 29, doi: [10.1088/0067-0049/199/2/29](https://doi.org/10.1088/0067-0049/199/2/29)
- Gianninas, A., Bergeron, P., & Ruiz, M. T. 2011, ApJ, 743, 138, doi: [10.1088/0004-637X/743/2/138](https://doi.org/10.1088/0004-637X/743/2/138)
- Hansen, B. M. S., Richer, H. B., Fahlman, G. G., et al. 2004, ApJS, 155, 551, doi: [10.1086/424832](https://doi.org/10.1086/424832)
- Heintz, T. M., Hermes, J. J., El-Badry, K., et al. 2022, ApJ, 934, 148, doi: [10.3847/1538-4357/ac78d9](https://doi.org/10.3847/1538-4357/ac78d9)
- Hollands, M. A., Littlefair, S. P., & Parsons, S. G. 2024, MNRAS, 527, 9061, doi: [10.1093/mnras/stad3729](https://doi.org/10.1093/mnras/stad3729)
- Holmberg, J., Nordström, B., & Andersen, J. 2009, A&A, 501, 941, doi: [10.1051/0004-6361/200811191](https://doi.org/10.1051/0004-6361/200811191)
- Kalirai, J. S. 2012, Nature, 486, 90, doi: [10.1038/nature11062](https://doi.org/10.1038/nature11062)
- Kalirai, J. S., Hansen, B. M. S., Kelson, D. D., et al. 2008, ApJ, 676, 594, doi: [10.1086/527028](https://doi.org/10.1086/527028)
- Kawka, A. 2020, in White Dwarfs as Probes of Fundamental Physics: Tracers of Planetary, Stellar and Galactic Evolution, ed. M. A. Barstow, S. J. Kleinman, J. L. Provencal, & L. Ferrario, Vol. 357, 60–74, doi: [10.1017/S1743921320000745](https://doi.org/10.1017/S1743921320000745)
- Kawka, A., Vennes, S., & Ferrario, L. 2020, MNRAS, 491, L40, doi: [10.1093/mnrasl/slz165](https://doi.org/10.1093/mnrasl/slz165)
- Kepler, S. O., Pelisoli, I., Koester, D., et al. 2015, MNRAS, 446, 4078, doi: [10.1093/mnras/stu2388](https://doi.org/10.1093/mnras/stu2388)
- . 2016, MNRAS, 455, 3413, doi: [10.1093/mnras/stv2526](https://doi.org/10.1093/mnras/stv2526)
- Kilic, M., Bergeron, P., Kosakowski, A., et al. 2020, ApJ, 898, 84, doi: [10.3847/1538-4357/ab9b8d](https://doi.org/10.3847/1538-4357/ab9b8d)
- Kilic, M., Moss, A. G., Kosakowski, A., et al. 2023, MNRAS, 518, 2341, doi: [10.1093/mnras/stac3182](https://doi.org/10.1093/mnras/stac3182)
- Kilkenny, D., O'Donoghue, D., Worters, H. L., et al. 2015, MNRAS, 453, 1879, doi: [10.1093/mnras/stv1771](https://doi.org/10.1093/mnras/stv1771)
- Kleinman, S. J., Kepler, S. O., Koester, D., et al. 2013, ApJS, 204, 5, doi: [10.1088/0067-0049/204/1/5](https://doi.org/10.1088/0067-0049/204/1/5)
- Koester, D. 2010, Mem. Soc. Astron. Italiana, 81, 921
- Koester, D., Dreizler, S., Weidemann, V., & Allard, N. F. 1998, A&A, 338, 612
- Koester, D., & Kepler, S. O. 2019, A&A, 628, A102, doi: [10.1051/0004-6361/201935946](https://doi.org/10.1051/0004-6361/201935946)
- Koester, D., Voss, B., Napiwotzki, R., et al. 2009, A&A, 505, 441, doi: [10.1051/0004-6361/200912531](https://doi.org/10.1051/0004-6361/200912531)
- Kraft, R. P. 1967, ApJ, 150, 551, doi: [10.1086/149359](https://doi.org/10.1086/149359)

- Külebi, B., Jordan, S., Nelan, E., Bastian, U., & Altmann, M. 2010, A&A, 524, A36, doi: [10.1051/0004-6361/201015237](https://doi.org/10.1051/0004-6361/201015237)
- Lanzafame, A. C., Distefano, E., Barnes, S. A., & Spada, F. 2019, ApJ, 877, 157, doi: [10.3847/1538-4357/ab1aa2](https://doi.org/10.3847/1538-4357/ab1aa2)
- Liebert, J., Bergeron, P., & Holberg, J. B. 2005, ApJS, 156, 47, doi: [10.1086/425738](https://doi.org/10.1086/425738)
- Limoges, M. M., Lépine, S., & Bergeron, P. 2013, AJ, 145, 136, doi: [10.1088/0004-6256/145/5/136](https://doi.org/10.1088/0004-6256/145/5/136)
- Lu, Y. L., Angus, R., Curtis, J. L., David, T. J., & Kiman, R. 2021, AJ, 161, 189, doi: [10.3847/1538-3881/abe4d6](https://doi.org/10.3847/1538-3881/abe4d6)
- Mamajek, E. E., & Hillenbrand, L. A. 2008, ApJ, 687, 1264, doi: [10.1086/591785](https://doi.org/10.1086/591785)
- Marigo, P., Cummings, J. D., Curtis, J. L., et al. 2020, Nature Astronomy, 4, 1102, doi: [10.1038/s41550-020-1132-1](https://doi.org/10.1038/s41550-020-1132-1)
- McCleaney, J., Tremblay, P.-E., Gentile Fusillo, N. P., et al. 2020, MNRAS, 499, 1890, doi: [10.1093/mnras/staa2030](https://doi.org/10.1093/mnras/staa2030)
- McCook, G. P., & Sion, E. M. 1999, ApJS, 121, 1, doi: [10.1086/313186](https://doi.org/10.1086/313186)
- Metcalfe, T. S., & Egeland, R. 2019, ApJ, 871, 39, doi: [10.3847/1538-4357/aaf575](https://doi.org/10.3847/1538-4357/aaf575)
- Moe, M., & Di Stefano, R. 2017, ApJS, 230, 15, doi: [10.3847/1538-4365/aa6fb6](https://doi.org/10.3847/1538-4365/aa6fb6)
- O'Brien, M. W., Tremblay, P. E., Gentile Fusillo, N. P., et al. 2023, MNRAS, 518, 3055, doi: [10.1093/mnras/stac3303](https://doi.org/10.1093/mnras/stac3303)
- O'Brien, M. W., Tremblay, P. E., Klein, B. L., et al. 2024, MNRAS, 527, 8687, doi: [10.1093/mnras/stad3773](https://doi.org/10.1093/mnras/stad3773)
- O'Donoghue, D., Kilkenny, D., Koen, C., et al. 2013, MNRAS, 431, 240, doi: [10.1093/mnras/stt158](https://doi.org/10.1093/mnras/stt158)
- Paxton, B., Bildsten, L., Dotter, A., et al. 2011, ApJS, 192, 3, doi: [10.1088/0067-0049/192/1/3](https://doi.org/10.1088/0067-0049/192/1/3)
- Paxton, B., Cantiello, M., Arras, P., et al. 2013, ApJS, 208, 4, doi: [10.1088/0067-0049/208/1/4](https://doi.org/10.1088/0067-0049/208/1/4)
- Paxton, B., Marchant, P., Schwab, J., et al. 2015, ApJS, 220, 15, doi: [10.1088/0067-0049/220/1/15](https://doi.org/10.1088/0067-0049/220/1/15)
- Prochaska, J. X., Hennawi, J. F., Westfall, K. B., et al. 2020, Journal of Open Source Software, 5, 2308, doi: [10.21105/joss.02308](https://doi.org/10.21105/joss.02308)
- Qiu, D., Tian, H.-J., Wang, X.-D., et al. 2021, ApJS, 253, 58, doi: [10.3847/1538-4365/abe468](https://doi.org/10.3847/1538-4365/abe468)
- Rebassa-Mansergas, A., Maldonado, J., Raddi, R., et al. 2023, MNRAS, 526, 4787, doi: [10.1093/mnras/stad3050](https://doi.org/10.1093/mnras/stad3050)
- Sahu, S., Gänscicke, B. T., Tremblay, P.-E., et al. 2023, MNRAS, 526, 5800, doi: [10.1093/mnras/stad2663](https://doi.org/10.1093/mnras/stad2663)
- Salaris, M., Serenelli, A., Weiss, A., & Miller Bertolami, M. 2009, ApJ, 692, 1013, doi: [10.1088/0004-637X/692/2/1013](https://doi.org/10.1088/0004-637X/692/2/1013)
- Salpeter, E. E. 1955, ApJ, 121, 161, doi: [10.1086/145971](https://doi.org/10.1086/145971)
- Shariat, C., Naoz, S., Hansen, B. M. S., et al. 2023, ApJL, 955, L14, doi: [10.3847/2041-8213/acf76b](https://doi.org/10.3847/2041-8213/acf76b)
- Sion, E. M., Oswalt, T. D., Liebert, J., & Hintzen, P. 1991, AJ, 101, 1476, doi: [10.1086/115779](https://doi.org/10.1086/115779)
- Skumanich, A. 1972, ApJ, 171, 565, doi: [10.1086/151310](https://doi.org/10.1086/151310)
- Temmink, K. D., Toonen, S., Zapartas, E., Justham, S., & Gänscicke, B. T. 2020, A&A, 636, A31, doi: [10.1051/0004-6361/201936889](https://doi.org/10.1051/0004-6361/201936889)
- Tian, H.-J., El-Badry, K., Rix, H.-W., & Gould, A. 2020, ApJS, 246, 4, doi: [10.3847/1538-4365/ab54c4](https://doi.org/10.3847/1538-4365/ab54c4)
- Tremblay, P. E., Bergeron, P., & Gianninas, A. 2011, ApJ, 730, 128, doi: [10.1088/0004-637X/730/2/128](https://doi.org/10.1088/0004-637X/730/2/128)
- Tremblay, P. E., Cukanovaite, E., Gentile Fusillo, N. P., Cunningham, T., & Hollands, M. A. 2019, MNRAS, 482, 5222, doi: [10.1093/mnras/sty3067](https://doi.org/10.1093/mnras/sty3067)
- Tremblay, P. E., Ludwig, H. G., Steffen, M., & Freytag, B. 2013, A&A, 559, A104, doi: [10.1051/0004-6361/201322318](https://doi.org/10.1051/0004-6361/201322318)
- Tremblay, P. E., Hollands, M. A., Gentile Fusillo, N. P., et al. 2020, MNRAS, 497, 130, doi: [10.1093/mnras/staa1892](https://doi.org/10.1093/mnras/staa1892)
- van Saders, J. L., Ceillier, T., Metcalfe, T. S., et al. 2016, Nature, 529, 181, doi: [10.1038/nature16168](https://doi.org/10.1038/nature16168)
- Vincent, O., Barstow, M. A., Jordan, S., et al. 2024, A&A, 682, A5, doi: [10.1051/0004-6361/202347694](https://doi.org/10.1051/0004-6361/202347694)
- Weidemann, V., & Koester, D. 1983, A&A, 121, 77
- Williams, K. A., Bolte, M., & Koester, D. 2009, ApJ, 693, 355, doi: [10.1088/0004-637X/693/1/355](https://doi.org/10.1088/0004-637X/693/1/355)
- Williams, K. A., Montgomery, M. H., Winget, D. E., Falcon, R. E., & Bierwagen, M. 2016, ApJ, 817, 27, doi: [10.3847/0004-637X/817/1/27](https://doi.org/10.3847/0004-637X/817/1/27)
- Xiang, M., & Rix, H.-W. 2022, Nature, 603, 599, doi: [10.1038/s41586-022-04496-5](https://doi.org/10.1038/s41586-022-04496-5)
- Zhao, J. K., Oswalt, T. D., Willson, L. A., Wang, Q., & Zhao, G. 2012, ApJ, 746, 144, doi: [10.1088/0004-637X/746/2/144](https://doi.org/10.1088/0004-637X/746/2/144)

APPENDIX

A. SYSTEMATIC SURFACE GRAVITY DIFFERENCES BETWEEN SPECTROSCOPY AND PHOTOMETRY

We find a systematic trend that the lowest surface gravities determined from spectroscopy deviate more strongly from those determined from photometry (see bottom panel of Figure 2, where there appears to be a correlated trend). Ignoring typical 3-D corrections for spectroscopic surface gravities (Tremblay et al. 2013) does not exaggerate this trend, and instead pushes the spectroscopic vs. photometric surface gravities into better agreement at lower spectroscopic surface gravities. The systematic offset also cannot be explained by the photometry being crowded or blended. Blended photometry would push the photometric surface gravities lower, not higher, thus bringing the spectroscopic and photometric surface gravities into better agreement. Double-degenerate binaries also cannot be invoked since they would broaden the lines, making the derived spectroscopic $\log g$ higher.

Instead, we find the systematic shift between surface gravities derived from photometry and spectroscopy at $\log g < 7.9$ can be explained statistically. Our formal spectroscopic fit uncertainties are 1.6 times larger on average than the uncertainties reported from photometry (see middle panel of Figure A1). We also expect the number of true $\log g < 8.0$ isolated white dwarfs should be small (e.g., O’Brien et al. 2024). Thus, we do not see white dwarfs where photometry and spectroscopy both return a low $\log g$; instead, white dwarfs with low spectroscopic surface gravities are, in fact, closer to $\log g = 8.0$.

To illustrate this, we generate a mock sample of 1000 white dwarfs with simulated true $\log g$ values similarly distributed to those from observed photometry in our wide WD+WD sample, with a strict cut at $\log g = 7.9$ (see first panel of Figure A1). Without the strict cut around $\log g = 7.9$, we are not able to reproduce the observed trend. We then introduce random errors into the measured photometric surface gravities ranging from 0.03 – 0.5 dex, which are drawn from the distribution of uncertainties on the photometric surface gravities reported in Heintz et al. (2022). We then require that the random errors introduced to the measured spectroscopic $\log g$ values reflect the relative empirical uncertainties (see Figure A1, middle panel). The resulting simulated distribution of $\log g$ differences between photometry and spectroscopy is compared to the observed sample in the right panel of Figure A1.

The simulated distribution captures the observed trend in the spectroscopic sample very well, and implies that most of the white dwarfs in our sample with spectroscopic $\log g < 7.9$ are, in fact, normal mass white dwarfs with surface gravities closer to $\log g = 8.0$. The larger scatter in spectroscopic surface gravities and the larger uncertainties are a consequence of the Balmer lines becoming weaker at lower effective temperatures (especially < 8000 K), and we recommend using the photometric $\log g$ in these cases, which should be more representative of the intrinsic surface gravity of the white dwarf. We note that there are some white dwarfs that have $\log g < 7.9$ from spectroscopy, but even smaller surface gravities from photometry (blue points in the bottom-left of the rightmost panel of Figure A1). These white dwarfs are probably close binaries that appear over-luminous in the Gaia CMD, and therefore have apparently lower surface gravities. For these objects, the spectroscopic surface gravities are a better estimate of the true value.

B. LDT AND SOAR SPECTRA WITH DA FITS

Here we tabulate all the spectroscopic parameters and spectral types determined through our LDT and SOAR follow-up observations. We also include a figure to the fits to each DA in our sample.

Table B1. Observed Spectral Types and Fitted Atmospheric Parameters from SOAR and LDT

Gaia DR3 ID	WDJ Name	G (mag)	Spectral Type	Instrument and Facility	SNR	UTC Date	T_{eff} (K)	$\log g$ (dex)
1100267237077449728	WDJ065350.43+635558.04	16.27	DC	LDT DeVeny	10	2020-01-20		
1141846540594232064	WDJ073615.22+794043.26	18.55	DC	LDT DeVeny	23	2021-04-14		
1141846540594232192	WDJ073615.19+794035.14	15.79	DA	LDT DeVeny	180	2021-04-14	20350 ± 240	8.01 ± 0.03
1165926910393567872	WDJ153401.77+101012.04	17.75	DA	LDT DeVeny	44	2020-08-11	7070 ± 80	7.75 ± 0.14

Table B1 *continued*

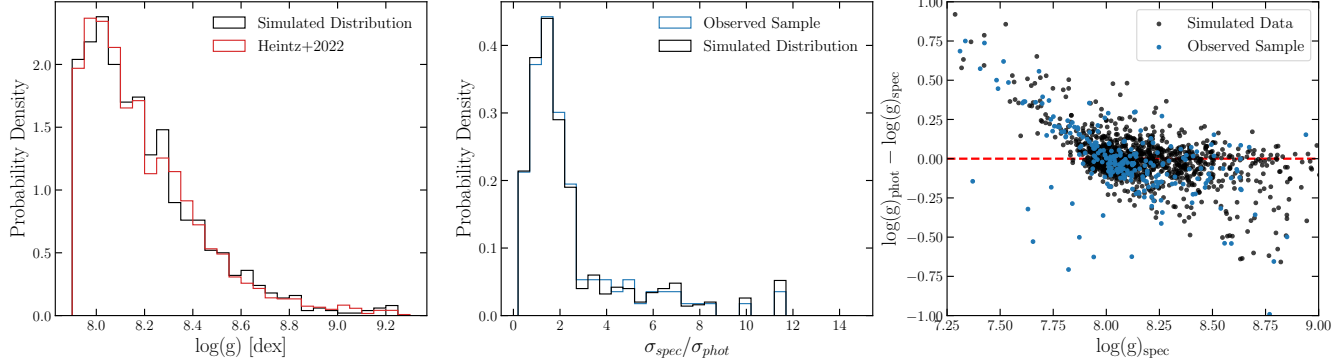


Figure A1. A simulated sample of 1000 white dwarfs to help illustrate the systematic trend seen in Figure 2. The left panel shows the distribution of the true $\log g$ values for our simulated sample (see text in Section A) and the sample of photometric $\log g$ values from Heintz et al. (2022), with white dwarfs with $\log g < 7.9$ removed. The middle panel shows the ratio of spectroscopic to photometric uncertainties for both the simulated sample and reported $\log g$ values from this work. The right panel shows the differences between the observed $\log g$ measurements from photometry and spectroscopy from this work on top of simulated measurements described in Section A.

Table B1 (continued)

Gaia DR3 ID	WDJ Name	G (mag)	Spectral Type	Instrument and Facility	SNR	UTC Date	T_{eff} (K)	$\log g$
1165926910393568384	WDJ153402.44+101024.24	18.09	DA	LDT DeVeny	32	2020-08-11	6410 ± 110	7.49 ± 0.30
1246692121126938240	WDJ135704.68+192133.34	16.85	DA	LDT DeVeny	98	2022-05-05	13820 ± 280	7.97 ± 0.03
1282448170543051520	WDJ144528.12+292124.29	17.36	DA	LDT DeVeny	36	2019-08-25		
1282448170543051648	WDJ144528.47+292132.07	14.51	DA	LDT DeVeny	245	2019-08-25	13040 ± 160	8.07 ± 0.03
1643897255075822976	WDJ151950.19+641540.48	17.79	DA	LDT DeVeny	43	2021-04-14	6160 ± 120	7.31 ± 0.31
1643897255075823104	WDJ151949.71+641534.74	18.42	DA	LDT DeVeny	25	2021-04-14		
1680759791146338048	WDJ122741.06+661224.33	18.08	DA	LDT DeVeny	34	2020-01-19	13890 ± 520	8.18 ± 0.07
1680759859865814656	WDJ122739.17+661224.39	17.97	DAH	LDT DeVeny	35	2020-01-19		
1682410707854900352	WDJ123030.22+675259.56	19.01	DC	LDT DeVeny	12	2020-01-19		
1682410776574377600	WDJ123029.22+675310.96	19.36	DC	LDT DeVeny	7	2020-01-19		
1829120747684237312	WDJ201836.79+212924.44	17.31	DA	LDT DeVeny	30	2019-08-25		
1829120747684239104	WDJ201836.72+212931.06	16.52	DC	LDT DeVeny	54	2019-08-25		
1840810854079992832	WDJ211531.38+253452.74	17.60	DA	LDT DeVeny	41	2019-10-02	8800 ± 110	8.13 ± 0.07
1840810858375964544	WDJ211531.58+253457.52	17.25	DC	LDT DeVeny	52	2019-10-02		
1874954641491354624	WDJ222301.60+220131.69	15.77	DA	LDT DeVeny	85	2020-08-11	19680 ± 240	8.45 ± 0.03
1874954645786146304	WDJ222301.71+220125.28	16.11	DA	LDT DeVeny	70	2020-08-11	14400 ± 440	8.27 ± 0.04
1911420636118031744	WDJ231941.38+342614.52	17.34	DA	LDT DeVeny	54	2019-08-25	16960 ± 200	8.13 ± 0.03
1911420636119326976	WDJ231941.48+342609.63	17.64	DA	LDT DeVeny	46	2019-08-25	14430 ± 470	8.17 ± 0.04
1932585268583421312	WDJ224133.59+412052.51	18.05	DA	LDT DeVeny	41	2019-10-02	9750 ± 120	8.11 ± 0.06
1932585302943159808	WDJ224134.34+412054.34	18.58	DA	LDT DeVeny	30	2019-10-02	11580 ± 210	8.67 ± 0.07
2080526555267049984	WDJ194530.33+465006.84	17.17	DC	LDT DeVeny	38	2019-10-02		
2080526555267050496	WDJ194530.35+465015.52	16.97	DA	LDT DeVeny	50	2019-10-02		
2142145179748734976	WDJ193124.32+570413.55	16.27	DA	LDT DeVeny	68	2019-08-25	16070 ± 290	8.59 ± 0.03
2142145385907166208	WDJ193124.43+570419.66	14.98	DA	LDT DeVeny	130	2019-08-25	24590 ± 300	8.24 ± 0.03
2150591795574568192	WDJ182519.30+553849.16	18.74	DC	LDT DeVeny	13	2021-06-12		
2150591799870095872	WDJ182518.67+553847.70	18.49	DC	LDT DeVeny	16	2021-06-12		
2214973561500636544	WDJ232117.26+692553.73	17.45	DC	LDT DeVeny	34	2020-09-22		
2214973771957744128	WDJ232117.29+692622.44	14.73	DA	LDT DeVeny	200	2020-09-22	20840 ± 250	8.03 ± 0.01
2238516205691628544	WDJ193744.39+590010.43	16.53	DA	LDT DeVeny	53	2019-08-25	9230 ± 110	8.12 ± 0.05
2238516240051369984	WDJ193745.94+590032.16	15.36	DA	LDT DeVeny	110	2019-08-25	12770 ± 150	8.01 ± 0.03
2310995767378550016	WDJ235343.05-362050.73	16.95	DC	SOAR Goodman	61	2018-08-08		
2310996145335674240	WDJ235344.03-362042.50	17.60	DA	SOAR Goodman	35	2018-08-08	6810 ± 80	8.27 ± 0.13

Table B1 continued

Table B1 (*continued*)

Gaia DR3 ID	WDJ Name	G (mag)	Spectral Type	Instrument and Facility	SNR	UTC Date	T _{eff} (K)	log g (dex)
2329764705742441216	WDJ232322.50-292921.55	19.14	DA	SOAR Goodman	20	2018-09-10	6740 ± 130	8.38 ± 0.23
2329764710037398528	WDJ232322.85-292916.58	18.47	DA	SOAR Goodman	36	2018-09-10	9190 ± 110	8.61 ± 0.04
2359214952893455872	WDJ010131.48-162909.12	18.44	DA	SOAR Goodman	49	2019-09-29	13320 ± 220	8.48 ± 0.03
2359214952893456000	WDJ010131.06-162908.14	18.68	DA	SOAR Goodman	33	2019-09-29	10100 ± 120	8.12 ± 0.04
2454507598448711296	WDJ012059.34-162248.18	18.80	DA	SOAR Goodman	25	2019-09-29	6280 ± 190	8.54 ± 0.33
2454507602744210432	WDJ012058.81-162246.57	15.84	DA	SOAR Goodman	206	2019-09-29	14930 ± 180	8.10 ± 0.01
2543653978300417024	WDJ002925.63+001552.72	18.47	DA	SOAR Goodman	29	2018-09-08	10190 ± 120	8.16 ± 0.06
2543654008364462848	WDJ002925.30+001559.78	19.54	DC	SOAR Goodman	13	2018-09-08		
2564851394251630848	WDJ013213.18+052633.00	16.30	DA	LDT DeVeny	72	2020-08-11	14570 ± 200	7.99 ± 0.03
2564945432560219008	WDJ013222.84+052925.09	18.21	DAZ	LDT DeVeny	33	2020-08-11		
2607475916712247168	WDJ230327.91-075504.82	18.26	DA	LDT DeVeny	41	2020-08-11	13690 ± 340	8.12 ± 0.05
2607475916712248064	WDJ230328.14-075457.97	18.26	DA	LDT DeVeny	41	2020-08-11	13140 ± 270	8.14 ± 0.06
2616210918121365760	WDJ222236.56-082806.01	17.19	DA	SOAR Goodman	29	2018-08-31	11840 ± 200	8.24 ± 0.06
2616210922414728960	WDJ222236.30-082807.97	16.54	DA	SOAR Goodman	41	2018-08-31	15640 ± 190	8.07 ± 0.03
2634608741244388096	WDJ230419.49-070149.84	19.03	DC	LDT DeVeny	16	2020-11-17		
2634608741244966016	WDJ230418.93-070124.51	17.07	DC	LDT DeVeny	120	2020-11-17		
2664365301168573824	WDJ231650.13+064123.48	18.61	DA	SOAR Goodman	18	2018-09-10	7970 ± 100	8.37 ± 0.13
2664365374183501312	WDJ231650.24+064128.42	16.08	DA	SOAR Goodman	100	2018-09-10	18150 ± 220	8.04 ± 0.01
2676567307551465088	WDJ215839.14-023916.44	17.09	DC	LDT DeVeny	9	2020-09-22		
2679752588442464768	WDJ215602.44-013829.07	17.63	DA	LDT DeVeny	42	2019-08-24	9140 ± 110	8.06 ± 0.07
2679765511998843520	WDJ215545.48-013455.69	17.73	DA	LDT DeVeny	36	2019-08-24	8690 ± 100	8.24 ± 0.08
2689069472018944256	WDJ210824.62-004133.72	19.65	DA	SOAR Goodman	10	2018-09-08	7360 ± 180	8.14 ± 0.28
2689069472018944896	WDJ210823.65-004130.83	18.29	DA	SOAR Goodman	37	2018-09-08	10730 ± 130	7.99 ± 0.03
2731501687319341568	WDJ224231.15+125004.99	16.35	DA	LDT DeVeny	85	2020-09-22	16240 ± 190	8.10 ± 0.03
2731502443233585280	WDJ224230.34+125002.42	16.61	DA	LDT DeVeny	74	2020-09-22	14380 ± 360	8.19 ± 0.03
2747684849212364928	WDJ002335.53+064325.89	18.45	DA	LDT DeVeny	16	2020-01-20	7620 ± 150	7.48 ± 0.29
2747684853507815552	WDJ002336.21+064320.90	17.42	DA	LDT DeVeny	45	2020-01-20	10410 ± 120	8.07 ± 0.06
2790494815860044544	WDJ010456.47+211958.87	17.70	DA	LDT DeVeny	26	2019-08-24		
2790494850219788160	WDJ010457.96+212017.54	17.80	DC	LDT DeVeny	21	2019-08-24		
282878984339974528	WDJ054015.76+610112.41	17.64	DA	LDT DeVeny	34	2021-03-23	12140 ± 240	8.22 ± 0.06
282878984339976320	WDJ054015.70+610123.34	18.32	DA	LDT DeVeny	19	2021-03-23	11300 ± 330	8.40 ± 0.12
2841680934336158976	WDJ232755.40+263824.46	17.58	DA	LDT DeVeny	59	2020-11-17	6620 ± 80	8.14 ± 0.15
2841680934336159104	WDJ232755.27+263821.32	18.30	DC	LDT DeVeny	22	2020-11-17		
2843077206728009472	WDJ230249.40+243028.69	17.95	DQ	LDT DeVeny	31	2020-11-17		
2843077211025217408	WDJ230250.40+243014.16	18.18	DA	LDT DeVeny	25	2020-11-17	6310 ± 140	7.54 ± 0.39
31047184711544832	WDJ030953.89+150511.53	18.43	DA	LDT DeVeny	30	2020-01-20	6560 ± 180	8.32 ± 0.38
31047257726638592	WDJ030953.95+150521.83	15.21	DA	LDT DeVeny	260	2020-01-20	22110 ± 270	8.07 ± 0.01
3284951791556594816	WDJ041840.44+055115.05	18.55	DB	LDT DeVeny	28	2020-01-20		
3284951791557832064	WDJ041840.69+055113.90	19.23	DA	LDT DeVeny	17	2020-01-20	11770 ± 400	8.26 ± 0.12
3330855616042214912	WDJ062210.56+110747.91	17.15	DA	SOAR Goodman	35	2018-12-30	13930 ± 440	8.63 ± 0.03
3330855616042218112	WDJ062208.96+110747.74	17.25	DA	SOAR Goodman	24	2018-12-30	16400 ± 360	8.49 ± 0.05
3334379344646313088	WDJ053724.80+073112.00	17.41	DA	SOAR Goodman	36	2018-12-30	6590 ± 80	8.46 ± 0.14
3334380100562482432	WDJ053720.93+073232.37	16.96	DC	LDT DeVeny	42	2020-01-19		
3404213863611804672	WDJ053834.31+223918.74	17.12	DC	LDT DeVeny	65	2020-11-17		
3404213863614488192	WDJ053834.52+223919.57	17.28	DA	LDT DeVeny	62	2020-11-17		
3562650151984291840	WDJ110021.77-160014.95	17.91	DC	LDT DeVeny	20	2021-04-14		
3562650151984292224	WDJ110022.76-160011.79	17.62	DA	LDT DeVeny	28	2021-04-14	6270 ± 260	8.17 ± 0.59
3603920492731480960	WDJ133651.76-162020.10	17.60	DA	LDT DeVeny	44	2021-04-14	25010 ± 390	8.19 ± 0.06
3603920595812980864	WDJ133652.21-162010.94	18.48	DA	LDT DeVeny	23	2021-04-14	11890 ± 440	8.70 ± 0.10
377231139432432384	WDJ005657.17+441018.64	15.94	DA	LDT DeVeny	91	2020-08-11	13260 ± 160	8.05 ± 0.03
377231345590861824	WDJ005656.68+441029.62	16.33	DA	LDT DeVeny	71	2020-08-11	11130 ± 130	8.05 ± 0.03
3823125109439975936	WDJ095618.10-035211.48	18.12	DA	LDT DeVeny	30	2020-01-19	9880 ± 120	8.32 ± 0.09
3823125109439978624	WDJ095617.48-035153.93	17.89	DC	LDT DeVeny	34	2020-01-19		

Table B1 *continued*

Table B1 (*continued*)

Gaia DR3 ID	WDJ Name	G (mag)	Spectral Type	Instrument and Facility	SNR	UTC Date	T_{eff} (K)	$\log g$ (dex)
3875651975353757440	WDJ101501.75+080611.24	17.49	DC	SOAR Goodman	26	2019-01-07		
3875652014008894720	WDJ101502.61+080635.70	15.92	DA	SOAR Goodman	107	2019-01-07	6730 ± 80	8.22 ± 0.04
3883615188318129536	WDJ101955.91+121631.53	15.76	DA	SOAR Goodman	67	2019-01-07	22790 ± 270	8.05 ± 0.03
3886617649631192320	WDJ101954.61+121718.03	16.87	DA	SOAR Goodman	34	2019-01-07	13020 ± 170	8.22 ± 0.04
3905533368502667520	WDJ121510.11+094836.37	17.77	DA	LDT DeVeny	34	2020-01-19	8510 ± 100	7.95 ± 0.10
3905534918987016576	WDJ121509.68+094847.14	17.92	DA	LDT DeVeny	34	2020-01-19	9960 ± 120	8.43 ± 0.07
4190500054845023488	WDJ195333.12-101954.85	17.26	DA	SOAR Goodman	38	2018-10-27	13700 ± 310	8.03 ± 0.04
428567401760258560	WDJ003230.15+600616.03	18.18	DC	LDT DeVeny	19	2020-01-19		
428567406061520896	WDJ003230.51+600620.08	18.88	DA	LDT DeVeny	10	2020-01-19	8160 ± 220	7.34 ± 0.38
4297600901227590272	WDJ194738.02+062510.15	18.87	DA	SOAR Goodman	17	2018-09-08	7990 ± 110	8.22 ± 0.15
4297600905539762432	WDJ194737.61+062508.48	18.63	DC	SOAR Goodman	21	2018-09-08		
4311973098757316608	WDJ185400.72+104854.69	18.17	DA	LDT DeVeny	43	2021-04-14		
4311973103092890752	WDJ185400.68+104851.56	18.01	DA	LDT DeVeny	45	2021-04-14	10210 ± 120	8.21 ± 0.07
4471738941493617408	WDJ181332.20+060412.61	17.26	DZ	LDT DeVeny	50	2019-08-24		
4471739010213094272	WDJ181330.47+060412.51	17.69	DA	LDT DeVeny	34	2019-08-24	6220 ± 130	7.70 ± 0.36
4500927474812609536	WDJ175137.69+151250.96	18.53	DA	SOAR Goodman	20	2018-09-10	7230 ± 120	8.51 ± 0.19
4500927504877462016	WDJ175137.51+151304.83	18.87	DC	SOAR Goodman	10	2018-09-10		
4848810205061914112	WDJ034011.79-420701.07	19.39	DC	SOAR Goodman	23	2019-01-09		
4848810205061914496	WDJ034011.52-420702.38	19.32	DA	SOAR Goodman	25	2019-01-09	6780 ± 140	8.77 ± 0.21
4855870439806768384	WDJ035012.19-383051.98	19.58	DC	SOAR Goodman	20	2018-12-31		
4855870439806768512	WDJ035012.13-383057.28	19.05	DA	SOAR Goodman	27	2018-12-31		
4940155500795290624	WDJ022440.28-461133.91	18.09	DAH	SOAR Goodman	32	2019-07-04		
4940155500795290880	WDJ022440.65-461140.65	17.41	DA	SOAR Goodman	52	2019-07-04	14010 ± 290	8.12 ± 0.03
5062948237833763840	WDJ024051.59-324837.30	17.52	DA	SOAR Goodman	42	2018-08-08	8380 ± 100	8.50 ± 0.05
5062948340912201088	WDJ024051.94-324814.09	17.59	DAH	SOAR Goodman	39	2018-08-08		
5131731035268115584	WDJ022556.26-175608.23	18.16	DA	SOAR Goodman	21	2019-07-05	6230 ± 160	8.19 ± 0.32
5131731039563630720	WDJ022556.45-175614.79	17.36	DZ	SOAR Goodman	44	2019-07-05		
5146493662498666624	WDJ022031.42-153248.98	18.45	DA	SOAR Goodman	32	2018-09-03	6620 ± 80	8.01 ± 0.13
5146493662498666752	WDJ022031.01-153248.08	18.17	DC	SOAR Goodman	42	2018-09-03		
5281331583776780416	WDJ071256.85-664407.33	19.24	DA	SOAR Goodman	24	2018-12-31	8560 ± 100	8.48 ± 0.07
5281331588075295232	WDJ071254.12-664409.71	19.20	DA	SOAR Goodman	25	2018-12-31	8830 ± 110	8.47 ± 0.07
5427657584803951232	WDJ092016.10-412709.51	17.58	DA	SOAR Goodman	33	2018-12-31	8370 ± 100	8.06 ± 0.06
5427657619159602944	WDJ092016.04-412702.01	17.59	DA	SOAR Goodman	32	2018-12-31	8320 ± 100	7.99 ± 0.06
5490676707920375936	WDJ072441.18-541935.42	19.45	DA	SOAR Goodman	19	2019-01-09	9640 ± 120	8.63 ± 0.09
5490676742283052800	WDJ072441.73-541935.33	19.20	DA	SOAR Goodman	23	2019-01-09	9060 ± 110	8.41 ± 0.07
5551794951535526144	WDJ064716.66-470744.24	18.98	DAH	SOAR Goodman	29	2018-12-31		
5551794951535528448	WDJ064715.56-470733.36	18.90	DAH	SOAR Goodman	30	2018-12-31		
5564028981196462336	WDJ065335.34-395533.29	15.35	DA	SOAR Goodman	56	2019-01-07	7220 ± 90	8.26 ± 0.05
5564029702750970112	WDJ065330.21-395429.12	15.92	DA	SOAR Goodman	38	2019-01-07	6400 ± 110	8.56 ± 0.18
5780478664144123264	WDJ162541.00-772112.71	18.13	DA	SOAR Goodman	44	2019-05-05	9350 ± 110	8.13 ± 0.04
5780478664144129152	WDJ162540.54-772104.20	18.55	DA	SOAR Goodman	31	2019-05-05	8510 ± 100	8.24 ± 0.06
6002657567182879104	WDJ152915.54-405524.74	18.52	DC	SOAR Goodman	28	2019-09-28		
6002657567182879616	WDJ152915.14-405526.00	18.08	DA	SOAR Goodman	43	2019-09-28	7980 ± 100	8.51 ± 0.05
6093462311215003776	WDJ135006.24-502534.22	18.07	DAH	SOAR Goodman	34	2019-07-04		
6093462315507278208	WDJ135006.04-502540.07	18.57	DA	SOAR Goodman	20	2019-07-04	6320 ± 160	8.23 ± 0.30
6458700145311223936	WDJ213406.66-575113.38	17.94	DA	SOAR Goodman	26	2018-09-09	7090 ± 90	7.97 ± 0.13
6458700149606803456	WDJ213406.86-575117.46	17.63	DC	SOAR Goodman	38	2018-09-09		
6590545195937635456	WDJ213136.44-345905.01	19.46	DA	SOAR Goodman	12	2018-09-09	7180 ± 190	8.64 ± 0.28
6590545195937636992	WDJ213136.47-345858.34	18.41	DA	SOAR Goodman	22	2018-09-09	7950 ± 100	8.08 ± 0.09
6642323156995855232	WDJ194406.24-534220.66	17.91	DA	SOAR Goodman	40	2019-05-05		
6642323156995855360	WDJ194406.22-534225.12	17.63	DA	SOAR Goodman	45	2019-05-05	13220 ± 260	8.55 ± 0.03
6898489884295407488	WDJ211507.40-074151.48	17.35	DA	SOAR Goodman	25	2018-10-27	8140 ± 100	8.21 ± 0.08
6898489884295412352	WDJ211507.42-074134.46	16.82	DA	SOAR Goodman	40	2018-10-27	10580 ± 130	8.41 ± 0.03

Table B1 *continued*

Table B1 (*continued*)

Gaia DR3 ID	WDJ Name	G (mag)	Spectral Type	Instrument and Facility	SNR	UTC Date	T_{eff} (K)	$\log g$ (dex)
733402121474544896	WDJ105707.88+301625.43	17.79	DC	LDT DeVeny	23	2021-04-14		
733402636870625152	WDJ105718.15+301823.17	18.56	DC	LDT DeVeny	13	2021-04-14		
867739936760402560	WDJ074723.48+243823.89	17.94	DA	LDT DeVeny	49	2020-11-17		
867740005479885184	WDJ074721.53+243847.89	18.57	DC	LDT DeVeny	24	2020-11-17		
961949666442453248	WDJ061725.77+433850.02	19.34	DC	LDT DeVeny	11	2020-01-19		
961949735161929728	WDJ061723.93+433846.21	19.19	DA	LDT DeVeny	13	2020-01-19	8240 ± 200	8.62 ± 0.27

NOTE—The S/N ratios tabulated here are calculated by taking the mean spectrum flux over spectrum error in a 200 Å window around 4600 Å

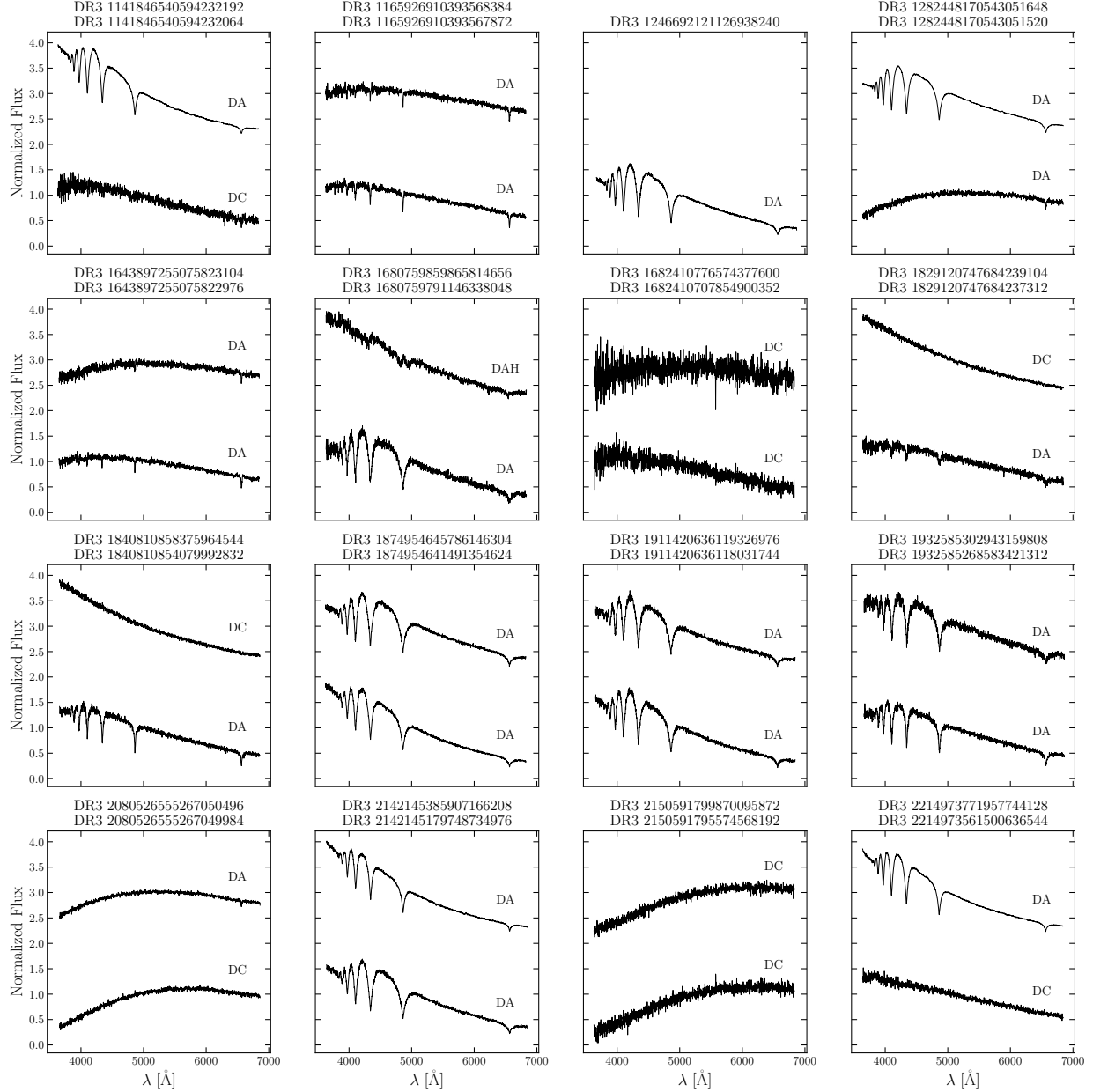
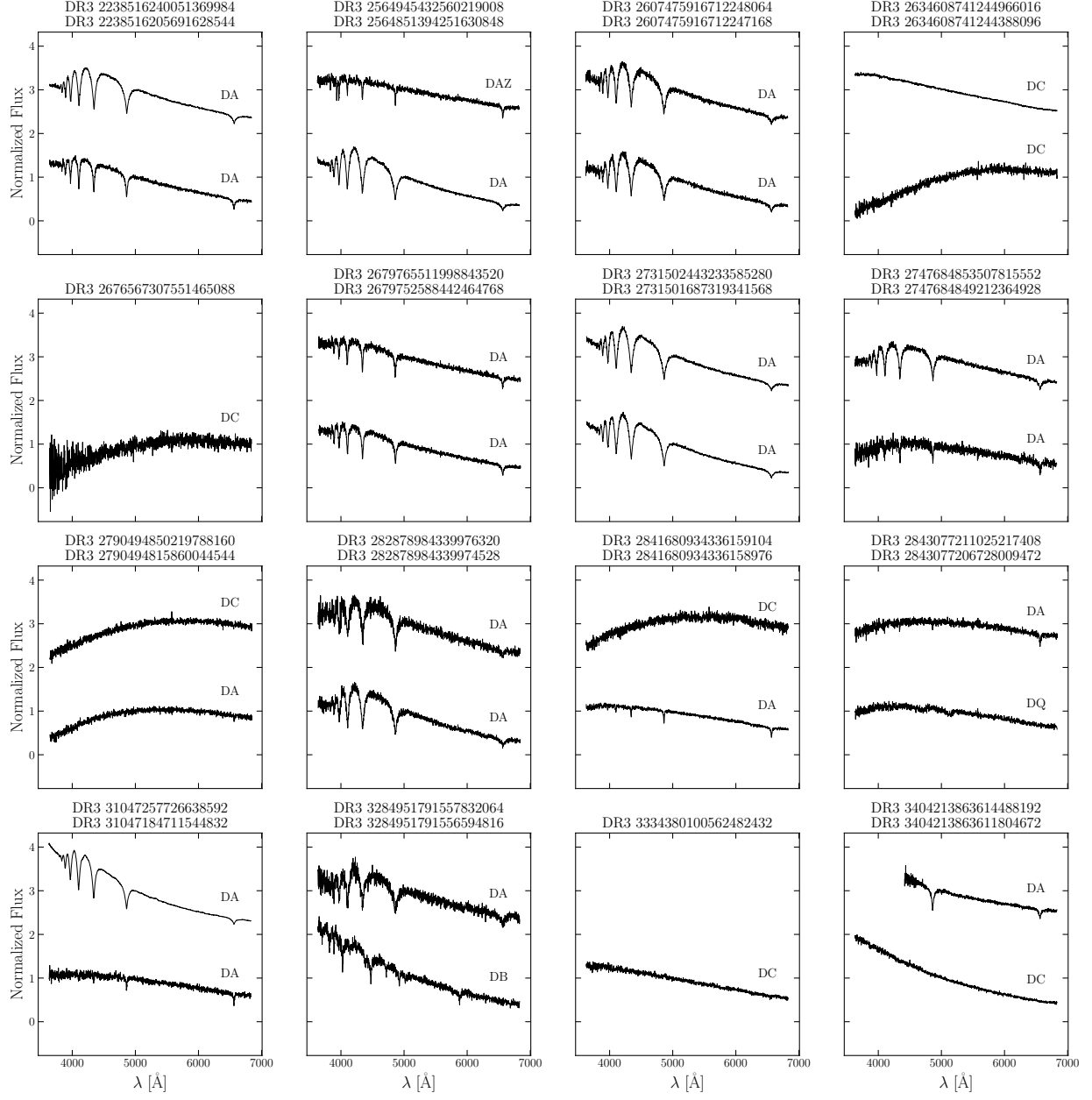


Figure B2. All newly observed white dwarf optical spectra with the DeVeny Spectrograph on the LDT.

**Figure B3.** Same as Figure B2, continued.

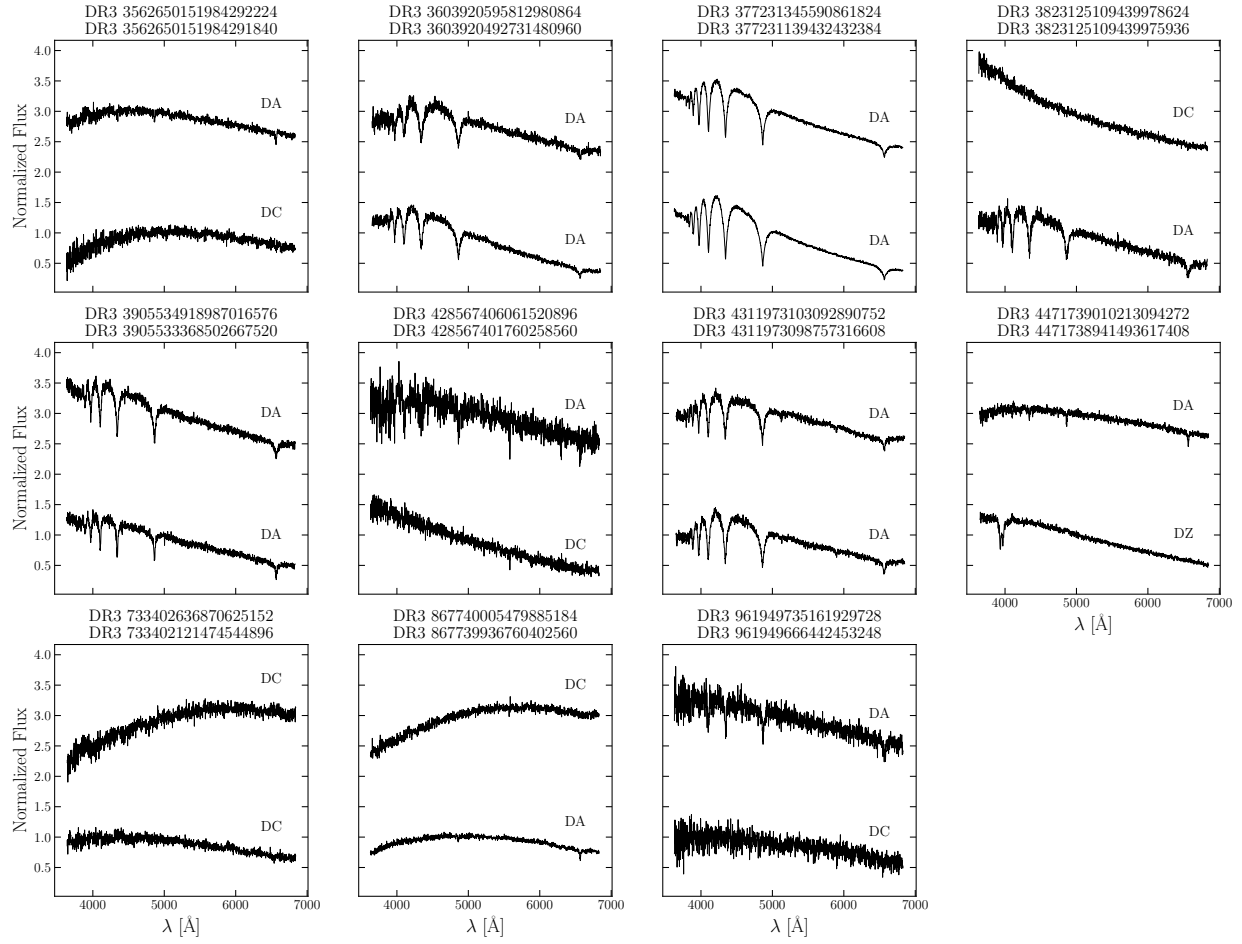


Figure B4. Same as Figure B2, continued.

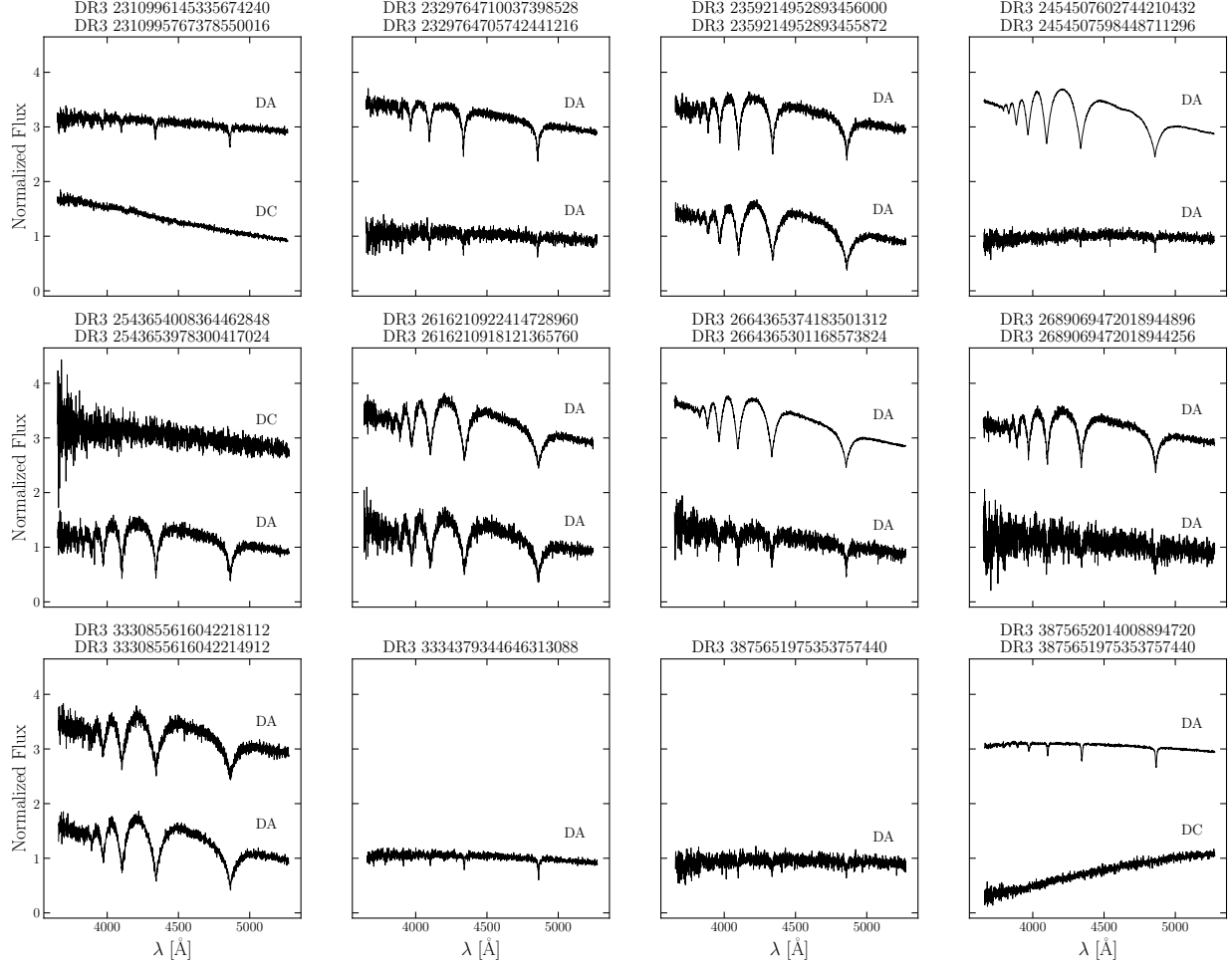


Figure B5. All newly observed white dwarf optical spectra with the Goodman Spectrograph on the SOAR telescope.

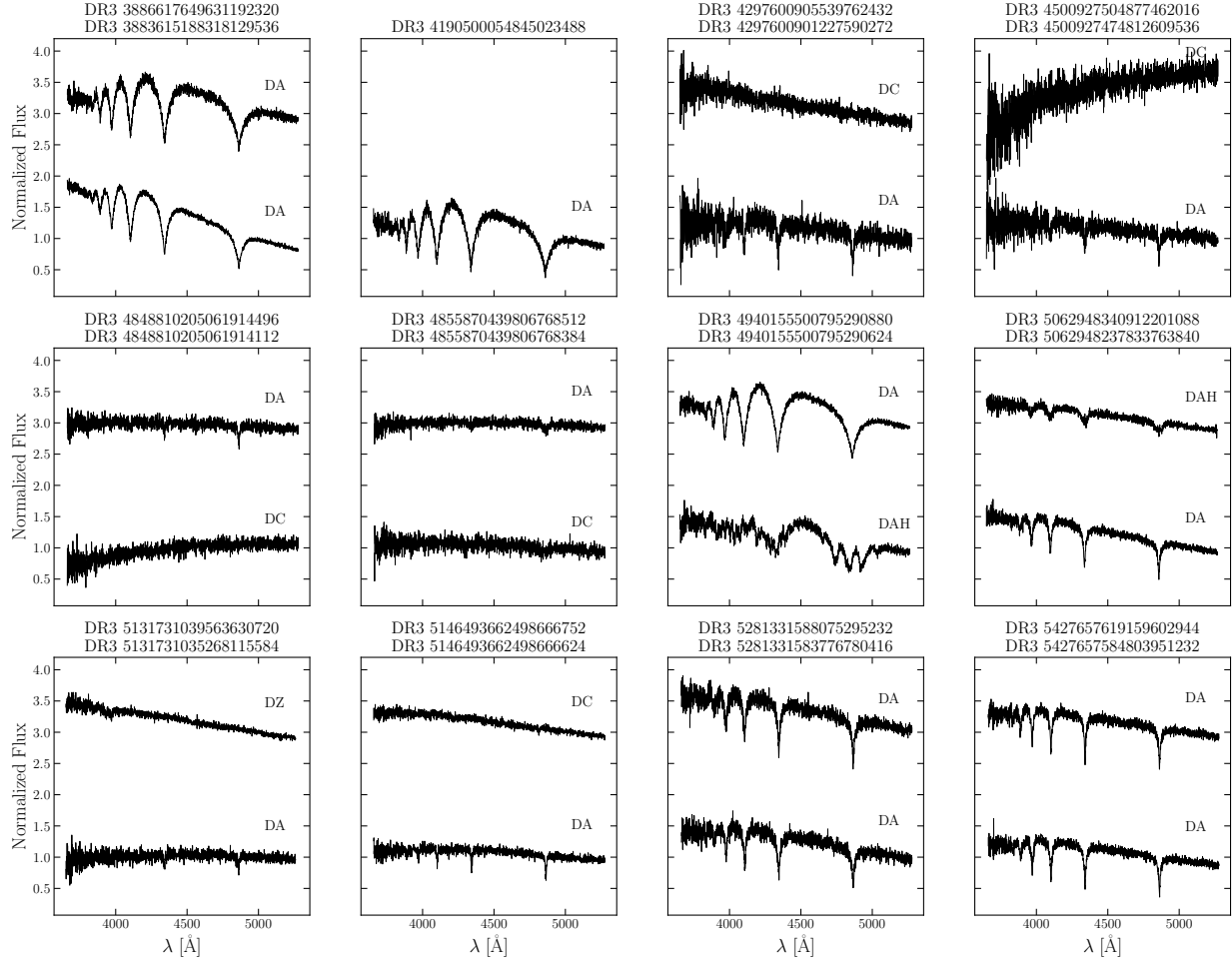


Figure B6. Same as Figure B5, continued.

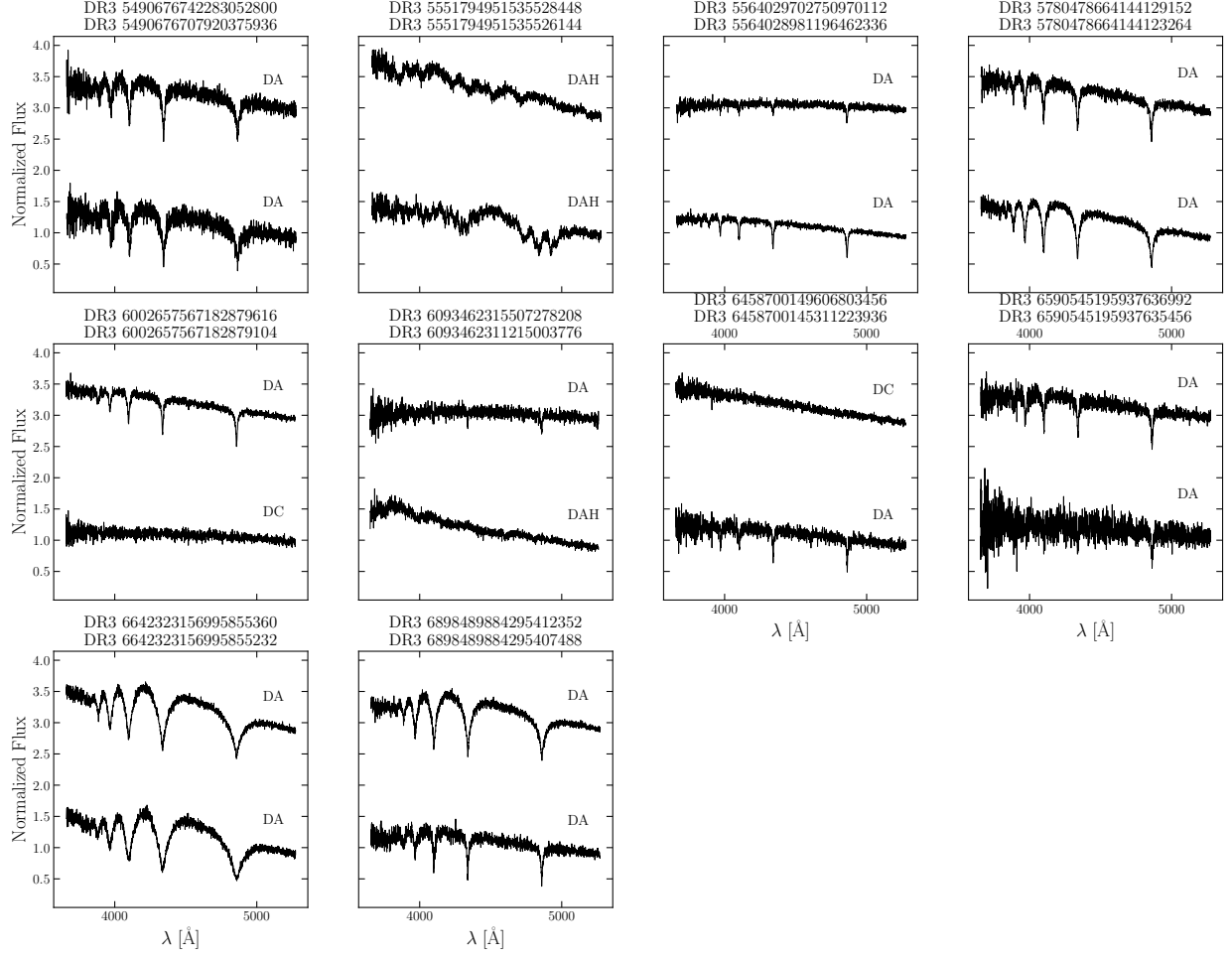


Figure B7. Same as Figure B5, continued.

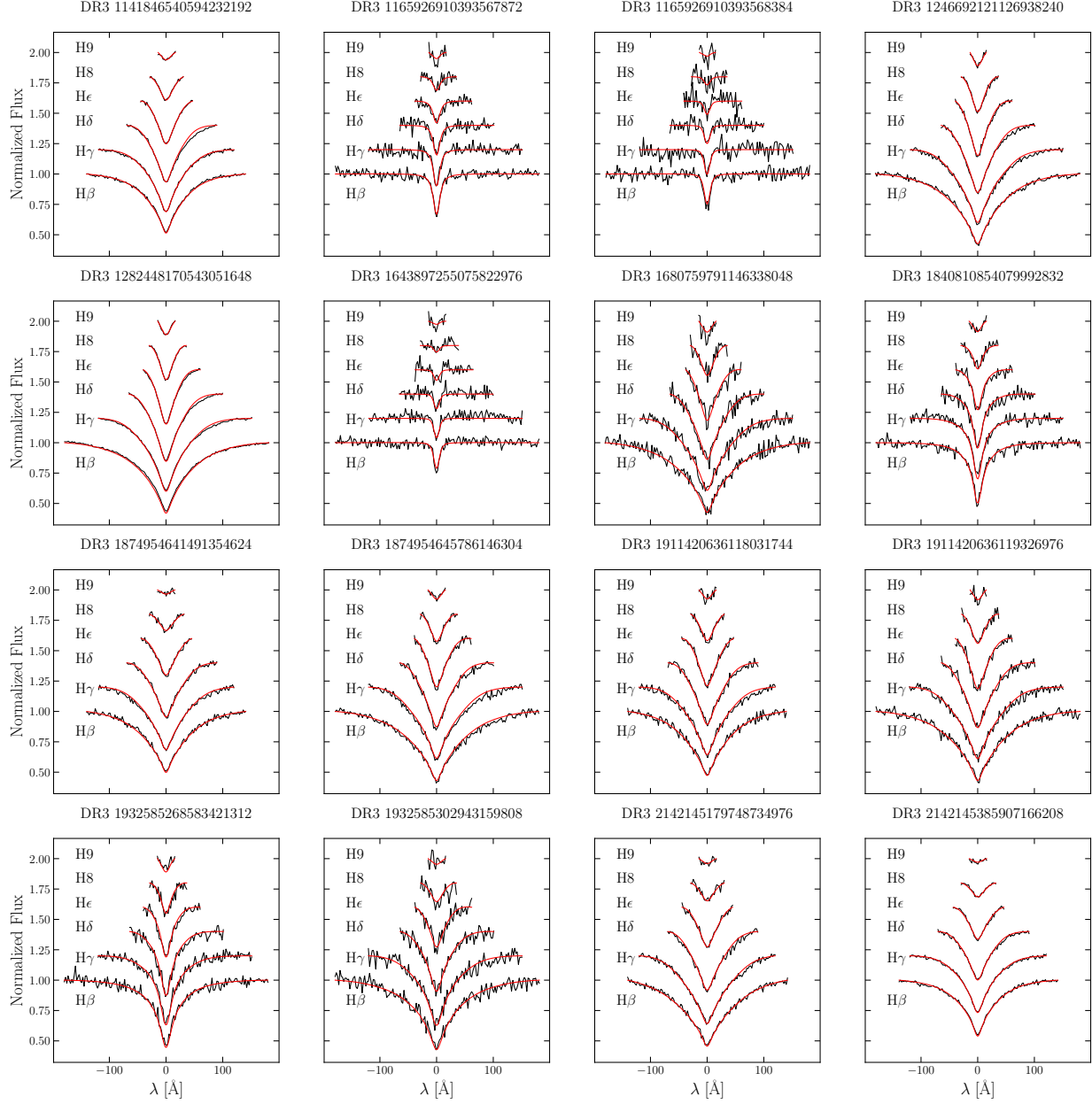


Figure B8. Spectral fits to the new DAs observed in this work (see Section 3.1), with observations in black and best-fit models in red.

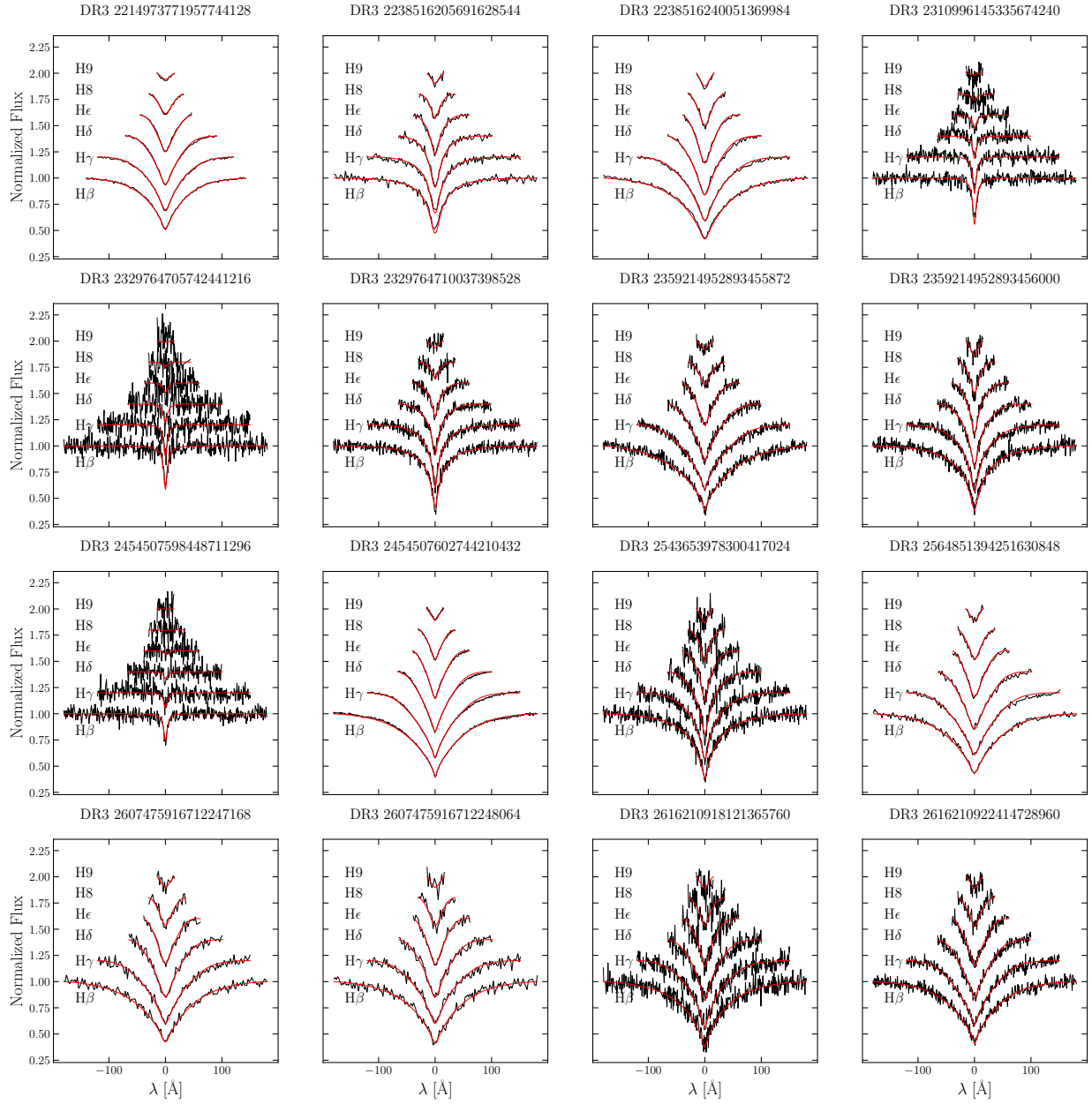


Figure B9. Same as Figure B8, continued.

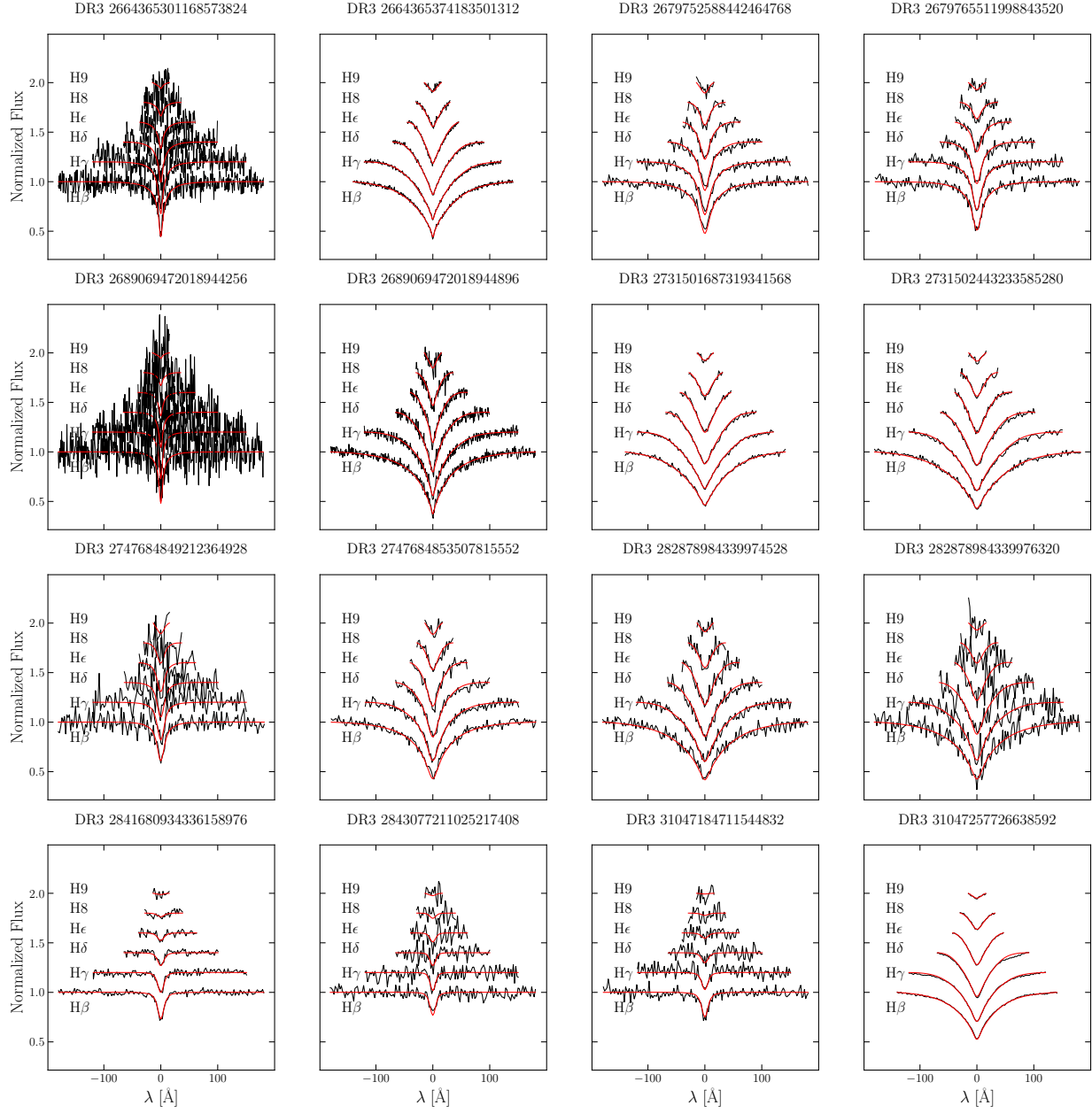
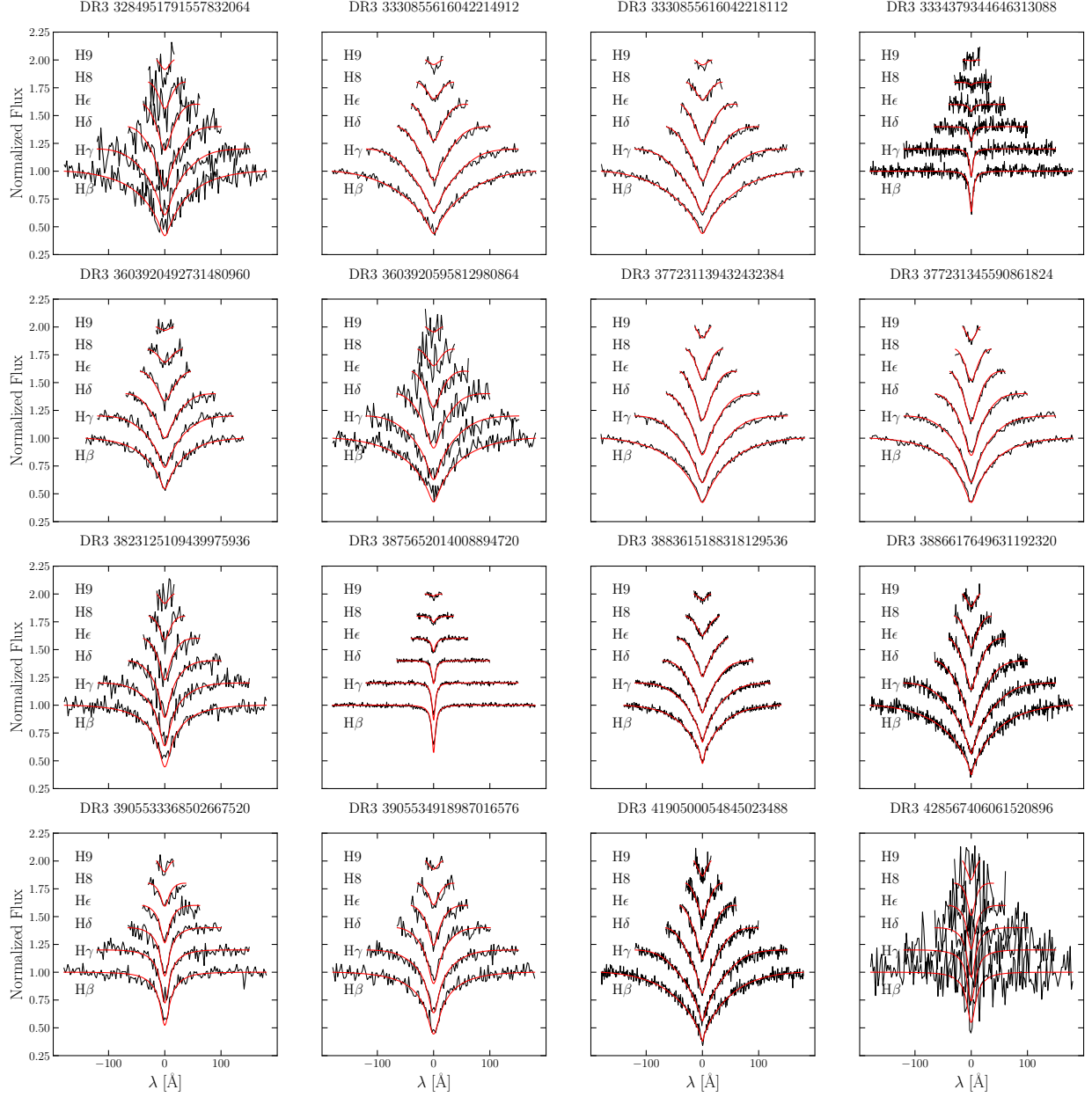


Figure B10. Same as Figure B8, continued.

**Figure B11.** Same as Figure B8, continued.

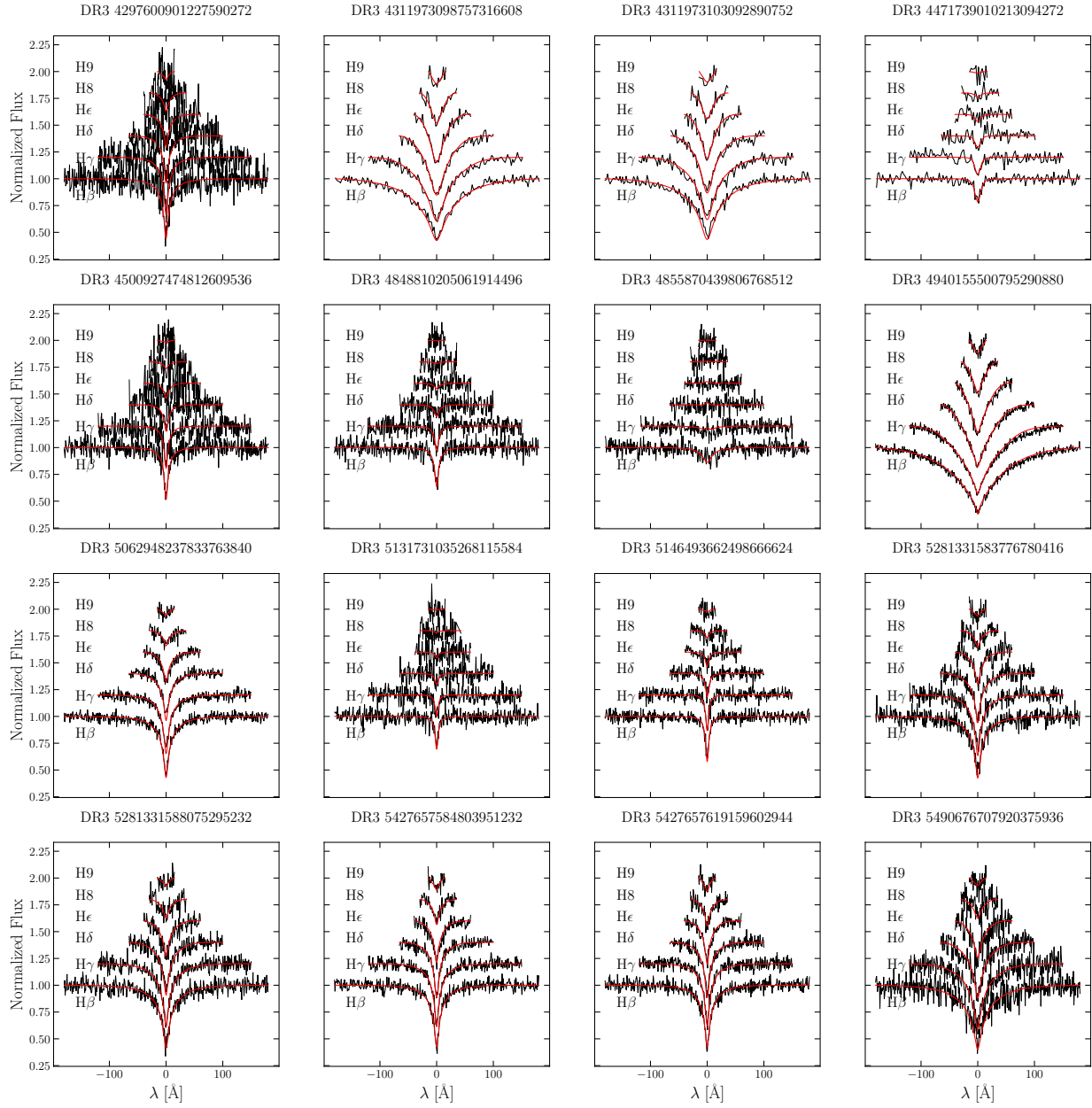
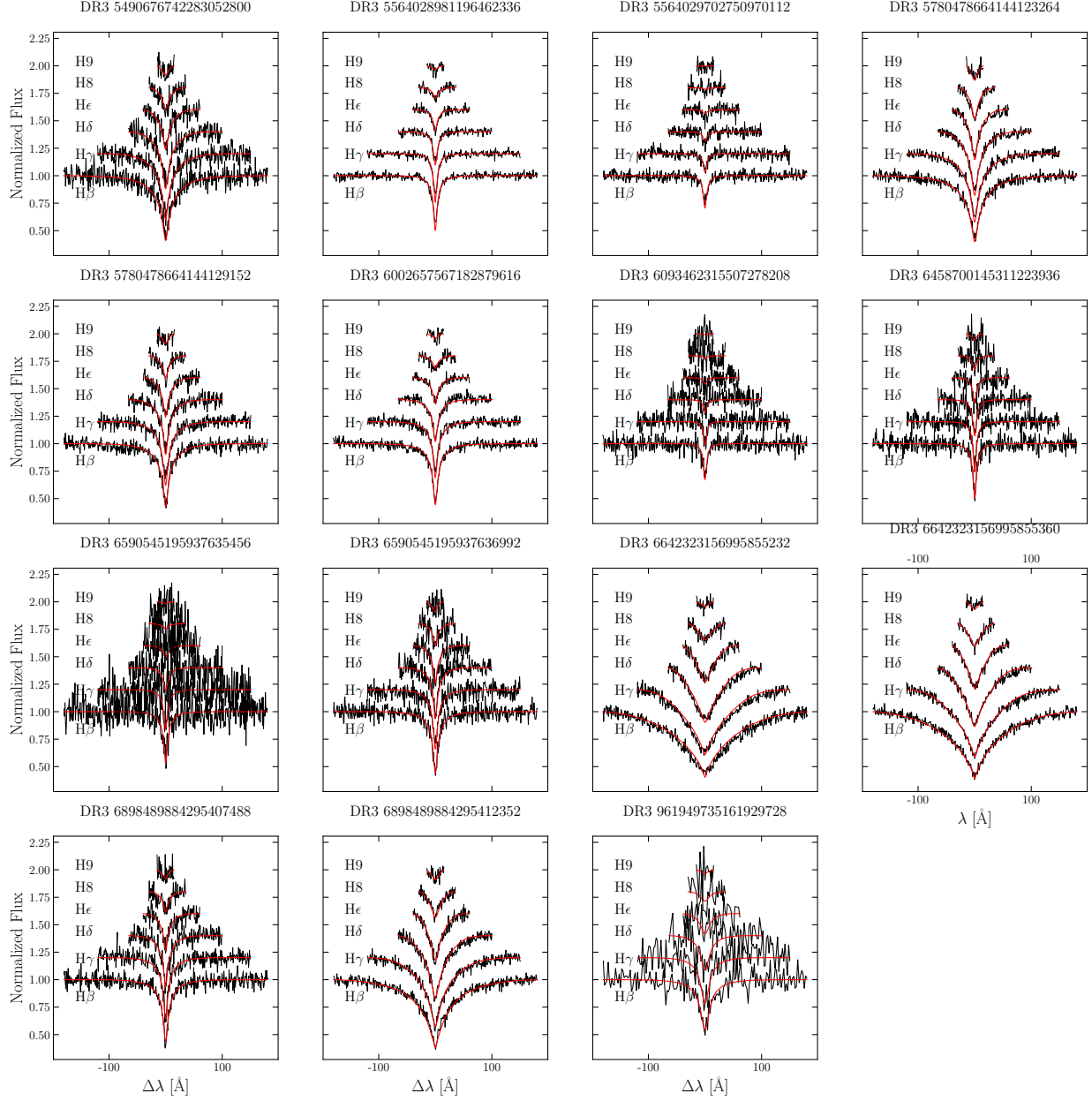


Figure B12. Same as Figure B8, continued.

**Figure B13.** Same as Figure B8, continued.**C. LITERATURE SPECTRAL TYPES AND SPECTROSCOPIC ATMOSPHERIC PARAMETERS**

Here we tabulate all the spectroscopic parameters and spectral types taken from previous works.

Table C2. Literature Spectral Types and Fitted Atmospheric Parameters

Gaia DR3 ID	WDJ Name	<i>G</i> (mag)	Spectral Type	Source	<i>T</i> _{eff} (K)	<i>log g</i> (dex)
1008929564913828224	WDJ085917.36+425031.67	18.93	DA	Baxter et al. 2014	10,020 ± 230	8.18 ± 0.13

Table C2 *continued*

Table C2 (*continued*)

Gaia DR3 ID	WDJ Name	G (mag)	Spectral Type	Source	T_{eff} (K)	$\log g$ (dex)
1008929569208837376	WDJ085917.24+425027.51	18.45	DA	Baxter et al. 2014	$11,150 \pm 250$	8.01 ± 0.08
1013776353903292928	WDJ084952.88+471249.58	16.87	DB	Baxter et al. 2014	$16,990 \pm 390$	7.84 ± 0.07
1013776353903293056	WDJ084952.49+471247.88	17.72	DA	Baxter et al. 2014	$11,230 \pm 260$	7.88 ± 0.07
1017810595208747776	WDJ085909.61+540953.17	19.92	DA	Gentile Fusillo et al. 2019		
1042071701528617856	WDJ084515.55+611705.79	17.17	DA	Tremblay et al. 2020	5470 ± 70	8.02 ± 0.02
1068909504756042112	WDJ091130.39+664502.03	19.06	DA	Tremblay et al. 2019	6900 ± 240	8.04 ± 0.43
1099325161772414208	WDJ070326.09+622251.24	15.65	DA	Gianninas et al. 2011	$17,140 \pm 260$	7.98 ± 0.05
1100655330324351616	WDJ065326.68+640342.05	16.49	DA	Gianninas et al. 2011	6000 ± 200	8.25 ± 0.43
1211378350265079808	WDJ153554.07+212506.58	17.22	DA	Limoges et al. 2013	6560 ± 110	8.59 ± 0.22
1218155666922068864	WDJ154403.20+234459.09	18.40	DA	Tremblay et al. 2019	9550 ± 110	7.95 ± 0.11
1218155666922071552	WDJ154403.27+234516.79	19.48	DC	Andrews et al. 2015		
1224799122336440576	WDJ154017.90+284457.36	20.12	DA	Kepler et al. 2015	7220 ± 110	7.70 ± 0.20
1238352149340737536	WDJ144921.38+205421.86	19.02	DAH:	Kilic et al. 2020		
1246997338682879104	WDJ140457.31+201246.15	18.74	DC	Kepler et al. 2015		
1247034339825405056	WDJ140237.20+201525.87	19.84	DC	Kepler et al. 2015		
1248152852388496896	WDJ134426.44+184931.13	18.03	DQ	Kleinman et al. 2013		
1302684712116023552	WDJ161229.09+233422.61	19.37	DA	Tremblay et al. 2019	$10,470 \pm 260$	8.20 ± 0.18
1332001785217988992	WDJ162555.28+375920.90	18.17	DA	Tremblay et al. 2019	7080 ± 90	8.27 ± 0.15
1337576648471644288	WDJ170356.78+330435.85	18.21	DA	Baxter et al. 2014	$11,310 \pm 260$	8.01 ± 0.07
1337576648471644800	WDJ170355.91+330438.49	18.78	DA	Tremblay et al. 2019	9500 ± 110	7.68 ± 0.13
1377401818623167104	WDJ153953.06+385520.65	19.01	DBZ:	Kepler et al. 2015		
1385162244707678720	WDJ160521.16+430435.93	14.80	DA	Gianninas et al. 2011	$37,550 \pm 560$	8.02 ± 0.05
1386046148977928832	WDJ160641.92+442027.32	20.14	DA:	Kepler et al. 2015		
1398291165161647872	WDJ155244.41+473124.05	19.11	DA	Baxter et al. 2014	$16,540 \pm 380$	7.91 ± 0.07
1398291165161649280	WDJ155245.20+473129.53	18.88	DA	Baxter et al. 2014	$18,770 \pm 430$	7.94 ± 0.07
1408135749896103936	WDJ170530.97+480310.27	14.53	DA	Gianninas et al. 2011	$14,170 \pm 290$	8.08 ± 0.05
1408135749896104192	WDJ170530.44+480312.36	14.39	DA	Gianninas et al. 2011	9250 ± 140	7.65 ± 0.06
1408293285000502400	WDJ165659.52+475648.83	20.07	DA	Kepler et al. 2016	8990 ± 110	8.02 ± 0.12
1448097259489385216	WDJ133441.32+255646.53	16.84	DA	Brown et al. 2007		
1448906637486139392	WDJ133611.40+273748.57	18.92	DC	Kleinman et al. 2013		
1450779346306149760	WDJ135834.67+263343.19	17.07	DA	Gentile Fusillo et al. 2019		
1459032658542428416	WDJ135228.45+342906.73	17.27	DB	Kepler et al. 2015	$11,600 \pm 140$	
1459033345737195008	WDJ135219.74+342853.09	19.42	DA	Kepler et al. 2015	6860 ± 80	8.21 ± 0.10
1463032819282938112	WDJ131421.52+305050.49	17.79	DA	Tremblay et al. 2019	$10,250 \pm 120$	8.02 ± 0.05
1463032819282938240	WDJ131421.73+305051.40	18.13	DA	Baxter et al. 2014	9170 ± 210	7.87 ± 0.07
1473687769854312192	WDJ132334.63+360912.03	18.64	DA	Tremblay et al. 2019	$10,040 \pm 120$	8.02 ± 0.09
1478574038183169024	WDJ141132.59+330836.81	20.00	DC:	Kepler et al. 2015		
1498271376679465600	WDJ141207.61+421627.40	16.01	DA	Gianninas et al. 2011	$16,020 \pm 280$	8.01 ± 0.05
1498271406743008640	WDJ141208.82+421624.85	18.28	DAH:	Tremblay et al. 2019		
1503769858234576128	WDJ134530.33+461741.85	19.34	DC	Kepler et al. 2016		
150577636388844160	WDJ042029.21+261755.39	18.38	DA	Kilic et al. 2020		
1521307274856035968	WDJ124038.89+383111.06	19.32	DA	Kepler et al. 2015	7370 ± 90	8.09 ± 0.12
1528594636063458688	WDJ125748.69+431913.77	19.62	DA:	Kepler et al. 2016		
1535762279348704000	WDJ121124.22+392427.63	19.47	DA	Tremblay et al. 2019	$10,840 \pm 160$	8.21 ± 0.08
1538128771968879616	WDJ122138.25+425933.21	18.84	DA	Tremblay et al. 2019	8260 ± 110	8.18 ± 0.15
1538128771968879616	WDJ122138.63+425934.13	19.88	DA	Gentile Fusillo et al. 2019		
1546811340415484800	WDJ120311.49+494832.30	18.82	DA	Tremblay et al. 2019	7100 ± 100	8.09 ± 0.17
1546811344714710912	WDJ120310.96+494850.91	17.35	DA	Andrews et al. 2015	$11,410 \pm 220$	8.12 ± 0.07
1552114525514355712	WDJ133820.22+473122.85	19.64	DA:	Kepler et al. 2016		
1564527844289256448	WDJ130955.74+550338.46	17.94	DA	Tremblay et al. 2019	8070 ± 100	8.12 ± 0.08
1564527878649314944	WDJ130954.23+550339.17	18.52	DA	Tremblay et al. 2019	8050 ± 100	7.89 ± 0.15
1568524088021418624	WDJ123940.38+503821.76	20.19	DA	Kepler et al. 2016	8430 ± 100	8.16 ± 0.13
1570271658673389568	WDJ125733.65+542850.45	16.69	DA	Tremblay et al. 2019		

Table C2 *continued*

Table C2 (*continued*)

Gaia DR3 ID	WDJ Name	G (mag)	Spectral Type	Source	T_{eff} (K)	$\log g$ (dex)
1574653689250360576	WDJ122717.44+563825.70	18.30	DA	Kepler et al. 2016	$15,680 \pm 190$	8.07 ± 0.02
1578748824604827648	WDJ130033.46+590406.83	17.93	DAH	Tremblay et al. 2019		
1578748858964566400	WDJ130035.20+590415.59	15.38	DA	Gianninas et al. 2011	$15,160 \pm 240$	8.00 ± 0.05
1579105719206817536	WDJ130606.76+592610.28	17.56	DC:	Kepler et al. 2016		
1580126370938935424	WDJ124238.82+612118.94	18.91	DA	Tremblay et al. 2019	7420 ± 160	7.87 ± 0.26
1580767149995407616	WDJ123156.08+573609.85	18.57	DA	Andrews et al. 2015	$11,190 \pm 230$	7.92 ± 0.08
1580767149995407744	WDJ123155.74+573611.47	17.91	DA	Andrews et al. 2015	$15,360 \pm 290$	8.01 ± 0.05
1593068623526189696	WDJ150746.82+520957.95	17.92	DAH	Dobbie et al. 2012		
1593068623526189824	WDJ150746.49+521002.04	17.11	DA	Dobbie et al. 2012	$17,600 \pm 210$	8.13 ± 0.02
1597058850006489856	WDJ154359.44+534456.73	20.46	DC:	Kepler et al. 2016		
1602106540386957184	WDJ153904.23+581115.83	17.66	DA	Tremblay et al. 2019	6930 ± 80	7.77 ± 0.13
16166875377576064	WDJ032026.89+111327.36	18.88	DA	Kilic et al. 2020		
16166875378033664	WDJ032026.96+111324.62	18.08	DA	Kilic et al. 2020		
1648851933643976448	WDJ164023.74+685424.81	16.49	DA	Gianninas et al. 2011	$18,770 \pm 300$	8.05 ± 0.05
1662446600351645184	WDJ134246.13+593830.72	19.81	DA	Kepler et al. 2016	$10,090 \pm 120$	8.79 ± 0.12
1675399225287958272	WDJ131022.04+611804.34	19.12	DC	Sion et al. 1991		
1678050701869897088	WDJ131520.69+652828.51	19.85	DA	Tremblay et al. 2019		
1678050873667756032	WDJ131520.60+652828.09	19.54	DA	Tremblay et al. 2019		
1682554091043762560	WDJ123647.43+682502.95	18.58	DC	Kepler et al. 2015		
1765847182089067008	WDJ214538.58+110619.69	19.93	DC	McCook & Sion 1999		
1767494804558717824	WDJ214208.53+132844.23	16.49	DA	Gianninas et al. 2011	7660 ± 130	8.09 ± 0.13
1781347890859073024	WDJ221019.65+203906.94	19.64	DA	Tremblay et al. 2019	$10,200 \pm 200$	7.41 ± 0.19
1875185779452781952	WDJ222426.91+231536.18	17.73	DA	Baxter et al. 2014	$10,740 \pm 250$	8.01 ± 0.07
187518588625938816	WDJ222427.07+231537.56	17.29	DA	Baxter et al. 2014	$13,200 \pm 290$	7.95 ± 0.07
1942154318286035328	WDJ233246.21+491709.15	18.88	DA	Tremblay et al. 2019	$18,200 \pm 340$	7.92 ± 0.06
2066035777984385664	WDJ204401.02+403014.24	15.44	DA	Andrews et al. 2015	$13,590 \pm 240$	8.00 ± 0.05
2066035777984385792	WDJ204400.72+403005.88	17.64	DAH	Andrews et al. 2015		
2274076297221555968	WDJ212657.66+733844.66	12.89	DA	Gianninas et al. 2011	$16,110 \pm 240$	7.97 ± 0.04
2317685436639994368	WDJ003918.81-310306.82	17.91	DA	Croom et al. 2004		
2364272573237917952	WDJ003230.41-175322.62	16.58	DA	Gianninas et al. 2011	$14,270 \pm 390$	7.94 ± 0.06
2416481783371550976	WDJ000734.82-160531.61	16.15	DA	Gianninas et al. 2011	$14,920 \pm 250$	7.93 ± 0.05
2422606780396753024	WDJ000022.54-105142.20	18.77	DA	Tremblay et al. 2011	8620 ± 110	8.06 ± 0.15
2429392661221943040	WDJ001440.69-075856.97	19.26	DC	Kilic et al. 2020		
2448158399834236928	WDJ000012.01-030831.10	19.87	DA	Gentile Fusillo et al. 2019		
2448482961923062400	WDJ000720.13-023456.24	18.79	DA	Kepler et al. 2016	6760 ± 80	7.43 ± 0.12
2469900005324049280	WDJ010904.22-104215.39	18.73	DA	Kilic et al. 2020		
2469900009618822656	WDJ010903.42-104214.15	16.60	DA	Kilic et al. 2020		
2477317211979980544	WDJ012824.94-082253.44	18.61	DA	Kleinman et al. 2013	6680 ± 80	7.79 ± 0.07
2477317211980446208	WDJ012824.99-082252.53	18.82	DA	Kleinman et al. 2013	6680 ± 80	7.79 ± 0.07
2482813425794003200	WDJ011728.64-043939.68	17.95	DC	McCook & Sion 1999		
2482813430089468160	WDJ011728.83-043938.41	17.87	DC	McCook & Sion 1999		
2490455242060072064	WDJ022443.44-024257.96	19.03	DA	Kilic et al. 2020		
2490455242060751360	WDJ022443.13-024255.30	19.09	DA	Kilic et al. 2020		
2499301496005547264	WDJ024443.74+011312.39	19.86	DA	Tremblay et al. 2019	8600 ± 240	7.99 ± 0.32
2501256839996606464	WDJ022733.10+005200.36	19.64	DA	Tremblay et al. 2019	$10,190 \pm 260$	8.40 ± 0.21
2501256839996606592	WDJ022733.16+005153.73	19.83	DA	Tremblay et al. 2019	9560 ± 110	8.07 ± 0.12
2512937609148915840	WDJ015343.13+042533.07	20.31	DA	Gentile Fusillo et al. 2019		
2588702614661788544	WDJ013910.70+144726.68	19.45	DA	Tremblay et al. 2019	9240 ± 240	8.85 ± 0.25
2629899631727265280	WDJ222542.67-011405.31	18.13	DA	Kilic et al. 2020		
2629899631727265920	WDJ222543.52-011359.51	19.21	DA	Kilic et al. 2020		
2644149993913188224	WDJ232658.90-002339.82	19.21	DA	Kleinman et al. 2013	7530 ± 90	8.13 ± 0.20
2644149993913188352	WDJ232659.23-002347.96	17.52	DA	Tremblay et al. 2011	$10,470 \pm 130$	8.08 ± 0.04
2645295921252503424	WDJ232115.34+010211.96	18.84	DA	Kilic et al. 2020		

Table C2 *continued*

Table C2 (*continued*)

Gaia DR3 ID	WDJ Name	G (mag)	Spectral Type	Source	T_{eff} (K)	$\log g$ (dex)
2645295955612242688	WDJ232115.70+010224.59	18.99	DA	Kilic et al. 2020		
2653032978419246208	WDJ223730.57-004754.70	19.67	DA	Kleinman et al. 2013		
2676566272464334720	WDJ215847.13-024024.42	17.15	DC	Tremblay et al. 2020		
2689364416012661760	WDJ212057.73-001810.62	18.27	DA	Tremblay et al. 2011	8630 ± 100	7.96 ± 0.10
2701318787466116352	WDJ213648.79+064320.22	18.10	DA	Kepler et al. 2015	$19,270 \pm 230$	8.02 ± 0.02
270359024105019680	WDJ222017.81+020342.88	18.77	DA:	Kepler et al. 2015		
2731184546933975040	WDJ222650.27+130832.75	17.71	DA	Gentile Fusillo et al. 2019		
2745919102257342976	WDJ000215.38+073359.56	17.72	DA	Andrews et al. 2015		
2745919106553695616	WDJ000216.18+073350.30	17.95	DAH	Andrews et al. 2015		
2749530521214502144	WDJ003310.14+074816.35	20.04	DA	Gentile Fusillo et al. 2019		
2749533025179314816	WDJ003247.88+074934.00	20.09	DA	Gentile Fusillo et al. 2019		
2751252493861856000	WDJ003424.36+102641.24	18.26	DA	Kepler et al. 2015	7110 ± 90	7.85 ± 0.06
2757867396332920576	WDJ233232.23+080230.00	18.19	DBA	Kepler et al. 2016	$36,500 \pm 440$	7.82 ± 0.04
2773334978019335040	WDJ235515.27+170806.73	18.23	DA	Andrews et al. 2015	$10,160 \pm 160$	8.31 ± 0.07
2773334982315549824	WDJ235515.44+170830.99	16.41	DB	Andrews et al. 2015	$21,470 \pm 440$	8.12 ± 0.03
2777645067895669376	WDJ005212.26+135302.04	17.81	DA	Baxter et al. 2014	$19,120 \pm 440$	7.94 ± 0.07
2777645067895669504	WDJ005212.72+135301.13	18.84	DA	Baxter et al. 2014	$10,880 \pm 250$	7.93 ± 0.07
2794800056333855232	WDJ003051.77+181053.88	18.82	DA	Andrews et al. 2015	$14,070 \pm 1050$	8.42 ± 0.18
2794800060629297152	WDJ003051.81+181046.16	18.85	DA	Andrews et al. 2015	$15,620 \pm 2930$	8.43 ± 0.35
2815944352131513088	WDJ225932.21+140439.28	16.59	DA	Gianninas et al. 2011	$28,340 \pm 410$	8.39 ± 0.05
2815944352131513472	WDJ225932.74+140444.25	18.63	DAH	Andrews et al. 2015		
2839231634746334848	WDJ231814.91+234509.51	19.44	DA	Kilic et al. 2020		
2839231634746334976	WDJ231815.26+234511.42	18.99	DC	Kilic et al. 2020		
2853079051690361088	WDJ000142.79+251504.18	18.86	DA	Tremblay et al. 2019	$18,470 \pm 220$	8.01 ± 0.03
2853985019206468352	WDJ000223.03+272358.26	17.68	DB	Kleinman et al. 2013	$16,760 \pm 200$	7.96 ± 0.06
2876148729784835584	WDJ001840.46+344147.72	19.43	DA	Kilic et al. 2020		
2876148734080688256	WDJ001839.94+344154.35	18.08	DA	Tremblay et al. 2019	7470 ± 90	7.94 ± 0.07
2879072503002076672	WDJ234526.50+350754.23	19.98	DA	Gentile Fusillo et al. 2019		
29406253782633216	WDJ011714.49+244021.58	19.70	DA	Tremblay et al. 2019	$17,670 \pm 590$	8.26 ± 0.10
3072961070640767488	WDJ082730.59-021620.14	17.99	DA	Andrews et al. 2015	$27,310 \pm 450$	8.49 ± 0.06
3072961074934467200	WDJ082730.73-021618.52	18.26	DA	Andrews et al. 2015	$27,860 \pm 490$	8.58 ± 0.07
3152007091864270336	WDJ075410.54+123947.46	18.85	DA	Andrews et al. 2015	$14,190 \pm 1070$	8.24 ± 0.12
3152007091867073152	WDJ075410.59+123945.62	18.90	DA	Andrews et al. 2015	$13,690 \pm 630$	8.31 ± 0.11
323375784298256896	WDJ012535.00+385047.07	19.11	DA	Tremblay et al. 2019	$13,570 \pm 410$	8.02 ± 0.06
32338868098140387840	WDJ051013.94+043838.43	14.23	DA	Gianninas et al. 2011	$21,550 \pm 320$	8.08 ± 0.04
32338868171156736768	WDJ051013.52+043855.13	15.38	DA	Gianninas et al. 2011	$12,010 \pm 190$	8.19 ± 0.05
3243842361760113408	WDJ033826.84-073155.40	16.49	DA	Kleinman et al. 2013	$15,640 \pm 190$	8.07 ± 0.02
3247469062209123072	WDJ032913.02-055520.75	18.51	DA	Kilic et al. 2020		
3247469130928600960	WDJ032911.76-055501.34	19.36	DA	Kilic et al. 2020		
3263351198434024576	WDJ033236.61-004918.41	18.21	DA	Baxter et al. 2014	$10,400 \pm 240$	8.03 ± 0.07
3263351202729621376	WDJ033236.87-004936.91	15.84	DA	Gianninas et al. 2011	$34,390 \pm 410$	7.80 ± 0.02
3301217592917972864	WDJ035454.20+074608.59	16.54	DA	Gianninas et al. 2011	$16,380 \pm 310$	7.87 ± 0.06
3310871201928485248	WDJ042641.73+141215.87	17.85	DA	Gianninas et al. 2011	$19,550 \pm 420$	8.88 ± 0.07
339492017717622016	WDJ022551.96+422803.52	17.31	DA	Gianninas et al. 2011	6320 ± 280	8.15 ± 0.56
3566532561902107648	WDJ111622.76-103516.10	18.99	DA	Kilic et al. 2020		
3566532561902107904	WDJ111623.74-103516.63	18.30	DA	Kilic et al. 2020		
3647484552174618368	WDJ141419.61-012217.76	18.62	DA	Kepler et al. 2015		
3647484556468720256	WDJ141418.87-012214.94	19.11	DA	Kepler et al. 2015	7900 ± 90	7.84 ± 0.05
3682458814461982592	WDJ125458.08-021837.75	16.64	DA	Koester et al. 2009	$15,930 \pm 280$	7.81 ± 0.07
3683519503881169920	WDJ124428.57-011857.85	13.99	DA	Gianninas et al. 2011	$24,480 \pm 370$	7.37 ± 0.05
3706830967160380416	WDJ123007.22+033856.12	18.91	DA	Tremblay et al. 2019	8630 ± 100	8.18 ± 0.12
3739031165907785216	WDJ133552.03+123709.07	16.30	DA	Kilic et al. 2020		
3739031268987206784	WDJ133552.15+123716.40	19.62	DA	Kilic et al. 2020		

Table C2 *continued*

Table C2 (*continued*)

Gaia DR3 ID	WDJ Name	G (mag)	Spectral Type	Source	T_{eff} (K)	$\log g$ (dex)
3745268523572692480	WDJ132814.32+163151.39	16.47	DA	Baxter et al. 2014	$20,000 \pm 460$	8.19 ± 0.07
3745268523573825792	WDJ132814.40+163150.79	17.42	DA	Gianninas et al. 2011	$18,800 \pm 320$	8.25 ± 0.05
3796545519645331584	WDJ112721.31-020837.66	16.39	DA	Gianninas et al. 2011	$25,180 \pm 400$	7.74 ± 0.05
3798238454018973056	WDJ112630.75+001958.86	19.84	DA:	Kepler et al. 2015		
3809511712378896384	WDJ105306.81+025027.98	19.07	DA	Tremblay et al. 2019	$12,330 \pm 410$	8.29 ± 0.10
3826588571067552256	WDJ095204.00-023044.14	18.08	DA:	Kepler et al. 2015		
3828044221382810752	WDJ094416.63-001855.53	19.59	DAH:	Kepler et al. 2015		
3835861439819152128	WDJ101359.85+030553.90	18.09	DA	Kilic et al. 2020		
3835866563715176192	WDJ101401.60+030550.42	18.03	DA	Kilic et al. 2020		
3845506012220187008	WDJ091659.86+032638.80	19.87	DA	Kepler et al. 2015	8420 ± 100	8.63 ± 0.13
3857475197016034432	WDJ104346.72+030318.45	19.14	DQ:PEC:	Kleinman et al. 2013		
3874412413432643328	WDJ100623.17+071154.30	18.64	DC	Kilic et al. 2020		
3874412413432647680	WDJ100623.08+071212.70	15.98	DA	Tremblay et al. 2019	9550 ± 110	7.96 ± 0.03
3900127108484055552	WDJ122319.59+050121.26	18.71	DA	Tremblay et al. 2019	8820 ± 110	8.25 ± 0.11
3902698243410506112	WDJ123313.51+082402.65	18.36	DQPEC	Kleinman et al. 2013		
3906688955223470080	WDJ120715.25+105337.88	18.42	DA	Kepler et al. 2015	$19,550 \pm 230$	8.14 ± 0.02
3906688955223834368	WDJ120715.45+105339.24	20.16	DA	Gentile Fusillo et al. 2019		
3920275276810355072	WDJ115937.82+134414.09	18.02	DA	Tremblay et al. 2019	9490 ± 110	7.99 ± 0.07
3920275276810355200	WDJ115937.83+134408.91	18.37	DA	Baxter et al. 2014	$16,400 \pm 380$	8.94 ± 0.07
3930720057454344960	WDJ125438.31+143228.61	16.93	DC	Kilic et al. 2020		
3930720263611949056	WDJ125437.34+143242.21	20.06	DC	Kilic et al. 2020		
3937174942327932544	WDJ131426.39+173228.40	18.43	DAH	Tremblay et al. 2019		
3937174946624964224	WDJ131426.84+173209.50	16.28	DA	Andrews et al. 2015	$12,530 \pm 210$	8.04 ± 0.05
3940068410255312768	WDJ131332.15+203039.39	17.86	DA	Baxter et al. 2014	$13,440 \pm 300$	8.30 ± 0.07
3940068414551140608	WDJ131332.57+203039.19	17.57	DA	Baxter et al. 2014	$13,210 \pm 290$	8.08 ± 0.07
3966161676608942976	WDJ113617.93+141812.47	18.63	DA	Tremblay et al. 2019	9360 ± 110	7.88 ± 0.10
3970693313784409344	WDJ112442.94+170513.95	18.54	DA	Tremblay et al. 2019	8100 ± 100	8.36 ± 0.11
3987906992950122112	WDJ104051.61+213033.75	20.11	DA	Kepler et al. 2015	7880 ± 100	8.12 ± 0.15
3989385561210153344	WDJ104459.57+215059.22	18.45	DA	Tremblay et al. 2019	7610 ± 90	7.82 ± 0.14
3993035733656088320	WDJ113136.33+234913.00	19.26	DAZ	Kepler et al. 2016	7440 ± 90	8.26 ± 0.06
41518658576469760	WDJ033912.60+143120.70	18.96	DA	Kilic et al. 2020		
42174998299513728	WDJ032538.35+150900.26	18.07	DC	McCook & Sion 1999		
4228388602763827584	WDJ204711.40+002127.73	17.17	DA	Tremblay et al. 2019	$14,390 \pm 180$	8.04 ± 0.02
4228388774562523264	WDJ204713.68+002203.96	18.24	DQ:M:	Kleinman et al. 2013		
4284122782775063552	WDJ182713.09+040346.79	13.92	DA	Gianninas et al. 2011	$14,350 \pm 220$	7.63 ± 0.05
42871199614383616	WDJ034411.48+150945.81	16.81	DA	Andrews et al. 2015	8300 ± 130	7.92 ± 0.09
42871268333859584	WDJ034410.90+151022.33	16.45	DC	Andrews et al. 2015		
4408166832745003904	WDJ161452.94+001632.49	18.86	DA	Tremblay et al. 2019	8120 ± 140	7.72 ± 0.21
4438147422454430464	WDJ161511.12+062155.66	20.24	DA	Gentile Fusillo et al. 2019		
4438147422454430464	WDJ161511.12+062155.66	20.39	DA	Gentile Fusillo et al. 2019		
4450425359563998720	WDJ160935.76+065509.73	17.65	DQ	Kepler et al. 2015		
4454302237563072768	WDJ155715.82+083022.64	18.67	DA	Tremblay et al. 2019	8160 ± 100	7.90 ± 0.14
4455997237817243776	WDJ155903.78+105614.51	18.75	DC:DA:	Kleinman et al. 2013		
4571341505129076992	WDJ170910.38+231933.58	17.31	DC	Kepler et al. 2015		
4592910074976281472	WDJ181331.21+324831.29	16.31	DA	Gianninas et al. 2011	7600 ± 120	7.76 ± 0.14
4592910105037219072	WDJ181335.45+324843.78	16.93	DA	Gianninas et al. 2011	6420 ± 220	7.61 ± 0.56
4598830738931385984	WDJ172929.26+291609.73	16.96	DA	Kilic et al. 2020		
4613612951211823104	WDJ031715.85-853225.56	14.75	DAH	Külebi et al. 2010		
5096781340192835712	WDJ041026.50-164142.57	16.36	DA	Kilkenny et al. 2015		
5096781344489104000	WDJ041024.93-164150.43	15.48	DA	O'Donoghue et al. 2013		
521406968152848640	WDJ015901.26+685800.45	18.48	DA	Kilic et al. 2020		
5436014972680358272	WDJ093659.94-372126.91	15.14	DA	Gianninas et al. 2011	7930 ± 110	7.87 ± 0.05
5436014972680358784	WDJ093659.79-372130.80	14.78	DQ	Sion et al. 1991		

Table C2 *continued*

Table C2 (*continued*)

Gaia DR3 ID	WDJ Name	G (mag)	Spectral Type	Source	T_{eff} (K)	$\log g$ (dex)
5649105922480851200	WDJ085550.71-263745.13	16.92	DA	McCook & Sion 1999		
5649105926779602432	WDJ085551.03-263750.20	16.77	DA	McCook & Sion 1999		
5762406957886626816	WDJ090217.30-040655.48	13.17	DA	Gianninas et al. 2011	$24,550 \pm 370$	7.89 ± 0.05
582509956042253312	WDJ084001.81+051628.41	17.97	DA	Tremblay et al. 2019	7770 ± 90	7.87 ± 0.09
5874024769842933760	WDJ145811.64-631733.46	17.51	DA	Gianninas et al. 2011	$10,270 \pm 150$	8.19 ± 0.05
5874024769842933760	WDJ145811.64-631733.46	16.83	DBA	Bergeron et al. 2011	$14,050 \pm 340$	7.96 ± 0.09
606938634805314816	WDJ090402.84+134915.01	16.10	DA	Andrews et al. 2015	9100 ± 140	7.78 ± 0.08
606938634805314944	WDJ090402.86+134911.33	16.60	DA	Tremblay et al. 2019	8170 ± 100	7.95 ± 0.04
627764274093469696	WDJ095427.16+195431.15	19.07	DA	Tremblay et al. 2019	7080 ± 190	7.74 ± 0.34
627764274093472896	WDJ095427.29+195448.38	19.02	DA	Tremblay et al. 2019	7310 ± 150	7.61 ± 0.28
630770819920096640	WDJ092513.50+160144.36	16.35	DA	Gianninas et al. 2011	$24,670 \pm 380$	8.35 ± 0.05
630770819920096768	WDJ092513.20+160145.62	17.33	DA	Finley & Koester 1997	$25,780 \pm 590$	9.04 ± 0.07
641625576666483584	WDJ094507.90+232723.59	17.26	DA	Gianninas et al. 2011	7240 ± 110	7.81 ± 0.09
641625576666484480	WDJ094508.66+232731.64	17.41	DA	Gianninas et al. 2011	6960 ± 120	8.15 ± 0.14
646608632082864256	WDJ094250.63+260059.85	14.62	DA	Gianninas et al. 2011	$70,580 \pm 1450$	7.94 ± 0.07
678526595643807872	WDJ083413.47+242600.78	20.19	DA	Gentile Fusillo et al. 2019		
6917231476602010240	WDJ210155.82-005745.10	17.80	DA:DC:	Kleinman et al. 2013	$25,910 \pm 350$	7.95 ± 0.04
695748628523317376	WDJ092212.25+292122.09	18.45	DA	Tremblay et al. 2019	7210 ± 130	7.87 ± 0.23
713277141676298240	WDJ085915.51+330637.62	18.77	DA	Baxter et al. 2014	$11,120 \pm 870$	7.75 ± 0.39
713277141676298496	WDJ085915.03+330644.69	18.18	DA	Baxter et al. 2014	$12,040 \pm 820$	8.05 ± 0.18
757911884925087104	WDJ111319.44+323817.72	18.79	DA	Tremblay et al. 2019	6920 ± 160	7.73 ± 0.30
757911988004305280	WDJ111322.54+323858.80	18.96	DA	Tremblay et al. 2019	7670 ± 180	8.63 ± 0.25
769201876477782144	WDJ114424.52+412847.35	18.67	DA	Tremblay et al. 2019	8590 ± 100	8.01 ± 0.07
769201880773377920	WDJ114424.57+412847.24	18.80	DA	Tremblay et al. 2019	8590 ± 100	8.01 ± 0.07
779305808516231552	WDJ104537.32+400535.94	18.90	DA	Tremblay et al. 2011	7760 ± 90	8.02 ± 0.10
779305808516517376	WDJ104537.43+400535.72	18.79	DA	Tremblay et al. 2019	7740 ± 90	7.99 ± 0.10
779767461666035584	WDJ104630.60+405905.62	18.89	DA	Tremblay et al. 2019	7220 ± 120	7.62 ± 0.22
782193985044906752	WDJ111020.98+451801.84	17.03	DA	Andrews et al. 2015	$19,000 \pm 300$	8.12 ± 0.05
782194019404645632	WDJ111016.68+451736.51	17.79	DA	Andrews et al. 2015	$13,700 \pm 370$	8.10 ± 0.06
795886439568266368	WDJ100244.89+360629.77	18.90	DA	Tremblay et al. 2019	$11,670 \pm 520$	8.29 ± 0.15
795886439568268032	WDJ100245.87+360653.50	18.99	DA	Andrews et al. 2015	$11,650 \pm 580$	8.26 ± 0.21
798602271945568256	WDJ092551.68+354000.58	17.67	DA	Tremblay et al. 2019	7060 ± 80	7.87 ± 0.10
804040108562044288	WDJ102141.29+394215.52	19.89	DA	Gentile Fusillo et al. 2019		
804040486519166976	WDJ102142.06+394225.50	20.24	DA	Gentile Fusillo et al. 2019		
837550886514384128	WDJ105449.90+530759.28	17.97	DA	Tremblay et al. 2019	$10,990 \pm 130$	7.94 ± 0.05
837550890811137664	WDJ105449.12+530715.35	17.65	DA	Andrews et al. 2015	$14,030 \pm 470$	8.07 ± 0.06
842498482680906496	WDJ110749.56+524651.01	18.31	DA	Tremblay et al. 2019	7090 ± 90	7.67 ± 0.17
842504358196167680	WDJ110751.05+524653.09	18.53	DA	Tremblay et al. 2019	6670 ± 220	8.11 ± 0.40
843874349685029504	WDJ111726.03+544305.01	20.42	DA	Kepler et al. 2016	7110 ± 140	7.79 ± 0.26
857095736490212608	WDJ105558.54+564543.62	19.52	DA	Kepler et al. 2016	8360 ± 100	8.36 ± 0.12
868275776880649856	WDJ073935.24+244505.20	17.45	DB	Kepler et al. 2015	$23,000 \pm 1500$	7.83 ± 0.02
879036662822100224	WDJ074853.08+302543.59	17.72	DAH	Tremblay et al. 2019		
893134841431510016	WDJ072147.37+322824.46	18.09	DC	Kleinman et al. 2013		
895406329374766208	WDJ073231.34+353543.74	20.00	DA	Gentile Fusillo et al. 2019		
906922545445227648	WDJ080410.00+355654.53	18.32	DA	Tremblay et al. 2019	7630 ± 90	8.17 ± 0.14
906922549740583808	WDJ080409.95+355659.11	18.70	DA	Tremblay et al. 2019	6930 ± 120	7.52 ± 0.23
925644685844771712	WDJ075412.09+430230.67	18.94	DA	Tremblay et al. 2019	$15,360 \pm 410$	7.83 ± 0.08
929001804082135168	WDJ080644.09+444503.19	18.22	DA	Baxter et al. 2014	$12,450 \pm 280$	7.99 ± 0.07
929001804082135296	WDJ080643.64+444501.43	18.76	DA	Baxter et al. 2014	$10,100 \pm 230$	7.96 ± 0.08